

A synchronization methodology for 3D offshore wind farm layout optimization with multi-type wind turbines and obstacle-avoiding cable network



Yan Wu ^{a, b, c}, Tianqi Xia ^c, Yufei Wang ^{a,*}, Haoran Zhang ^{c, d}, Xiao Feng ^b, Xuan Song ^e, Ryosuke Shibasaki ^c

^a School of Chemical Engineering and Environment, China University of Petroleum (Beijing), 18 Fuxue Road, Changping, Beijing, 102249, China

^b School of Chemical Engineering and Technology, Xi'an Jiaotong University, 28 Xianning West Road, Xi'an, Shaanxi, 710049, China

^c Center for Spatial Information Science, The University of Tokyo, 5-1-5 Kashiwanoha, Kashiwa-shi, Chiba, 277-8568, Japan

^d School of Business, Society and Engineering, Mälardalen University, Västerås, 721 23, Sweden

^e SUSTech-UTokyo Joint Research Center on Super Smart City, Department of Computer Science and Engineering, Southern University of Science and Technology (SUSTech), Shenzhen, China

ARTICLE INFO

Article history:

Received 11 March 2021

Received in revised form

24 August 2021

Accepted 13 December 2021

Available online 17 December 2021

Keywords:

Offshore wind farm

Cable network

Seabed terrain

Multi-type wind turbine

Meta-heuristic algorithms

ABSTRACT

Offshore wind farms are increasingly becoming the focus of clean sources market because of the huge energy potential and fast-maturing technology. The existing researches normally optimize the wind turbine layout and two-dimensional cable routing independently. This work focuses on the synchronization optimization of site selection of the offshore wind farm, three-dimensional wind turbine layout and three-dimensional cable network routing based on meta-heuristic algorithms and geographic information systems. Several practical issues, i.e., restricted areas, power generation, cable network and energy loss, are taken into consideration. A two-layer model is proposed. The outer layer model is for the site selection and the wind turbine layout optimization. The inner layer model is for the obstacle-avoiding cable routing optimization. In this stage, the seabed terrain is considered for the first time. The proposed integrated model is complex and non-convex. Thus, a hybrid method including an improved ant colony optimization combined with genetic algorithm, dual-simplex method and Kruskal algorithm is proposed to search the solution more efficiently. The initialization stage of the hybrid method is improved from random assignment to directional assignment. The directional solution is obtained by the widely used genetic algorithm. A case study based on a real offshore wind farm is established to prove the effectiveness of the proposed methodology. The results show an over one million dollars increase in annual benefit compared with conventional methods.

© 2021 Elsevier Ltd. All rights reserved.

1. Introduction

Wind energy is a promising renewable source with cost-competitive around the world and has achieved rapid and high-quality development in the last 20 years. As reported by global wind energy council (GWEC), the global total installed capacity reaches 650 GW in 2019, the new installation is 60 GW with a 19% growth compared to 2018. New installations in the offshore wind market passed the milestone of 6 GW. It is expected that over 355 GW of new capacity will be added in five years. That is nearly 71 GW of new installations each year until 2024 [1]. Compared with

onshore wind farms, offshore wind farms have more advantages, i.e., large offshore areas, enormous energy potential and less impact on landscape. For the design of an offshore wind farm, a crucial stage is the design of the initial layout with wind turbines (WTs), substations and cable networks. There are two main trends in current researches on this point: (1) the construction and development of the model involving more issues, such as annual energy production (AEP), the cost of energy (COE), electricity system (cable connection and energy loss), noise, risks, uncertainty and social consideration; (2) the application of the improved algorithms to solve models.

Regarding the models describing the problem of offshore wind farm layout (OWFL), energy production and the cost of energy are the most important issues that should be taken into consideration. Because the total investment of an offshore wind farm is huge, even

* Corresponding author.

E-mail addresses: wangyufei@cup.edu.cn, yufei-wang@outlook.com (Y. Wang).

a small improvement in the layout would save lots of money. Lackner and Elkinton [2] modeled the energy production as a function only related to the positions of WTs. Pérez et al. [3] established a nonlinear programming (NLP) model to maximize the energy production of offshore wind farms considering wake loss described as Jensen model. The model was tested by a real offshore wind farm, observing an 3.52% increase in annual power production. Recently, Brogna et al. [4] developed a new engineering wake model with good accuracy to solve the problem of wake modeling in complex terrain. A systematic comparison of eight optimization algorithms is carried on and the results showed that random search and local search are the best algorithms to solve the model. Generally, the terrain of the offshore wind farm is flat, so it is not necessary to use such a complicated model in our research. Furthermore, according to the study of Archer et al. [5], among six popular analytical models of the wake loss, i.e., Jensen [6], Larsen [7], Frandsen [8], Bastankah & Porté-Agel (BPA) [9], Xie and Archer (XA) [10] and geometric mode (GM) [11], Jensen and XA performed best overall. Therefore, Jensen model is used in this study. Besides the velocity deficit model mentioned above, the added turbulence intensity is another important factor of wake loss [12]. It is associated with the fatigue loads of the wind turbine. Several models have been proposed by Crespo and Hernández [13], Frandsen and Thøgersen [14], etc. However, according to the best knowledge of the authors, added turbulence intensity has not been considered in the most published models for the layout problem of offshore wind farms. In 2015, Fischetti et al. [15] proposed a mixed-integer linear programming (MILP) model to maximize the power generation of onshore and offshore wind farms under different wind scenarios considering the constraint of the distance between WTs. Additionally, a model considering wind uncertainty and opportunistic condition-based maintenance was developed by Song et al. [16]. Maienza et al. [17] constructed a life cycle cost model for floating offshore wind farms including capital cost (CAPEX), operation and maintenance cost (O&M-OPEX) and decommissioning cost (DECEX), which provides a good foundation for wind farm assessment.

On the other hand, cable connection costs account for a large part of the overall investment and should be considered. The optimization of the cable connection is mostly studied independently because it is by itself a complex mathematical problem [18]. The problem is widely described as a minimum spanning tree (MST) problem [19–23]. Peng et al. [20] adapted Prim algorithm to find the best connection of cables. Prim algorithm is a classic method for solving MST, as well as Kruskal algorithm. Hou et al. [21] used an adaptive particle swarm optimization-minimum spanning tree (PSO-MST) algorithm to solve the problem after obtaining several sub-regions of the wind farm by fuzzy C-means clustering algorithm. Cerveira et al. [24] proposed different integer linear programming models and computed the optimal solutions for three real projects considering energy losses. Wędzik et al. [25] simultaneously optimized the cable network and cable cross-sections considering energy loss by mixed-integer linear programming (MILP) method. Besides, cable connection problems can be also described as a the minimum Steiner tree problem. Wu et al. [26] optimized the cable network of an onshore wind farm by GeoSteiner algorithm and obtained shorter connections. Fischetti and Pisinger [27] solve the cable routing problem with no-cross restrictions, connection limits at the substation, and obstacles. They used Steiner point to model obstacles and applied additional Steiner points to deal with curvy cable connections. Recently, Klein and Haugland [28] presented an integer linear programming (ILP) for cable routing considering obstacles on the offshore wind farm. Jiang et al. [29] developed a fuzzy evidential reasoning method for

submarine cable routing considering maritime safety. A three-layer decision-making framework was established to derive the belief rule base and to obtain the optimal routing. However, most of the studies mentioned above are separated from the optimization of power generation. Moreover, the research on three-dimension (3D) cable routing considering the seabed topography is rare. A synchronization model combines WTs layout optimization and three-dimension cable network layout optimization is needed to achieve wind farm construction more efficient and economical.

Considering the complexity of the wake loss model and the power model, the OWFL problem is non-linear and extremely non-convex [30] which means the model involves many sub-optimal solutions. Meta-heuristic algorithms are widely used to solve the OWFL model. Genetic algorithm (GA) is used in more than 75% of wind farm layout optimization studies [31]. Chen et al. [32] applied a nested GA to solve the model considering different hub height WTs in a two-dimension area and analyzed different wind conditions. Gao et al. [33] proposed a multi-population genetic algorithm (MPGA) to maximize power generation with minimum investment cost for a hypothetical offshore wind farm located in Hong Kong. Hou et al. [34] optimized OWFL with a wake loss model using particle swarm optimization (PSO) algorithm. The variables in the model are discrete. In 2016, Pookpunt and Ongsakul [35] used a binary PSO to optimize wind farm spacing, position, sizing, hub height simultaneously. Ant colony optimization (ACO) is used by Eroğlu and Seçkiner [36] for searching the wind farm layout with more energy production. The results showed that ACO performed better than GA applied in the study of Kusiak and Song [37]. Sri-kakulapu and Vinatha [38] presented an approach combined ACO and multiple traveling salesmen problems (MTSP) to optimize the OWFL considering cable connection. Simulated annealing algorithm (SAA) [39] can be also applied for OWFL, as well as coral reefs optimization algorithm [40], cuckoo search algorithm [41], and informed mutation operator algorithm [42]. Note that Zhang et al. [43] proposed an effective approach based on ACO to solve a complex MINLP model for the production schedule. The approach meets the characteristics of the model proposed in this work and it has not been used in the OWFL problem. Therefore, the improved ACO in this article refers to their approach.

For the site selection of the wind farm, geographic information system (GIS) is usually applied. A GIS-based model, considering economic, social and environmental factors, was proposed for wind farm site suitability analysis by Ayodele et al. [44]. Interval type-2 fuzzy analytic hierarchy process (AHP) is used to solve the issues of uncertainty, vagueness and inconsistency in wind farm site selection decision making. Castro-Santos et al. [45] presented a methodology using GIS spatial analysis for the site selection of a floating offshore wind farm. The restrictions of environmental protected regions, navigation restricted areas (obstacles), bathymetry, ports and shipyards was analyzed in their study to guide the location planning of a wind farm. Actually, the restriction areas have critical influence on the WTs layout and submarine cable routing when the wind farm is close to them. However, the application of GIS has not been found in the layout optimization stages for an offshore wind farm, and there are few studies on the offshore wind farm layout considering restriction areas.

In general, the limitations of current researches on OWFL can be summarized as the following four points.

- (1). Most of the researchers independently optimized WTs layout and cable routing, and there is no synchronous optimization model for multiple sub-problems.
- (2). The practical factors, which are taken into consideration, are not comprehensive enough and still need to be improved.

- (3). Cable layout stays on the 2D plane, there is a lack of a 3D cable routing method based on GIS data.
- (4). For the complex model that integrates multiple sub-problems, an effective algorithm more suitable for the characteristics of the model has not yet been developed.

To make up for these shortcomings, this study addresses developing an integrated model describing 3D WTs layout and cable network based on meta-heuristic algorithms and GIS. The main contributions are:

- (1). An integrated two-layer model is proposed to achieve the synchronization optimization of the site selection, WTs & substations layout and 3D obstacle-avoiding cable connections in an offshore wind farm.
- (2). Several practical factors, such as restricted areas (obstacles), wake loss, multi-type WTs, cable type selection, cable investment, energy loss and operation & maintenance cost, are taken into consideration.
- (3). GIS-based seabed terrain is involved innovatively in the methodology.
- (4). A hybrid method combining GA-IACO, dual-simplex method and Kruskal algorithm is developed to solve the problem powerfully.

2. Mathematical formulations

2.1. Problem definition

A representative offshore wind farm is basically composed of a certain scale of wind turbines and power transmission systems. Wind turbines generally refer to wind turbines and wind turbine foundations (submarine support). At present, most existed offshore wind farms use high-voltage alternating current transmission systems including cables, offshore substations and onshore substations. Cables are generally divided into output cables and array cables. The proposed model is set as optimizing the layout of offshore multi-type WTs, the 3D submarine cable network topology considering seabed topography, and the wind farm site selection in a given sea area considering several obstacle areas simultaneously. The obstacle area may be a fishery, a harbor, or a nature reserve. It is determined according to the specific conditions of different sea areas. The given area is gridded, only one WT can be placed on a grid. If the grid is in the obstacle area, the WT cannot be located on it, besides, the cable also cannot be laid in the obstacle area. The length between every two vertexes is the sum of all the three-dimensional lengths of each two adjacent vertexes on the path. The synchronization model has two layers. The outer layer optimizes the location of the WT array and the relative locations of WTs, offshore substations and onshore substations with the maximum annual economic benefit considering the investment, operation cost and power loss. The inner layer model optimizes the cable network with the shortest length, power generation and power loss. The model can be described in Fig. 1.

2.1.1. Input

- (1). Coordinates and sizes of the given area and obstacle areas.
- (2). Parameters of different types of WTs and the number of WTs of each type.
- (3). Parameters of the offshore substation and onshore substation.
- (4). Wind data and other parameters of the given area.
- (5). Gridded bathymetry data of the given area.
- (6). Parameters of different types of submarine cable data.

2.1.2. Determine

- (1). Locations of WTs, the offshore substation and the onshore substation.
- (2). Cable network topology of the wind farm.
- (3). Types and number of cables in the connection network.
- (4). Annual economic benefit, power output for each WT, investment and operation cost, power loss during the transmission.

There are several reasons for establishing a two-layer model. The proposed optimization is comprehensive and has many sub-problems. There are thousands of variables in the proposed LP model for the optimization of the cable network. For the LP model, the dual-simplex method can find the global optimal solution in a short time, while the efficiency of using heuristic algorithms to solve such problems is lower than the former. Besides, other sub-models, such as the wake loss model and power loss model, have strong nonlinearity and the heuristic methods are more suitable for solving. Therefore, solving the proposed two-layer model can obtain the relative optimal solution of the selection and the layout within a reasonable time, and can obtain the optimal solution of the cable network quickly. Using a two-layer model can reduce the difficulty of modeling and solving a single-layer model. Suitable algorithms also can be used to solve different models to increase the quality of the solution and the efficiency of the calculation.

The proposed model has three advantages. Firstly, the two-layer model describes a comprehensive wind farm layout optimization problem, and it is easy to be solved by suitable algorithms. Secondly, the wake loss model is a 3D model and considers the hub height of different types of wind turbines. It meets the actual needs of practical engineering. Thirdly, the 3D cable network model considers the seabed terrain, obstacles, power loss and cable selection simultaneously. The proposed model is not only suitable for offshore wind farms, but can also guide the 3D layout design of onshore wind farms and floating wind farms.

2.2. Wind speed model

Wind speed is an essential component for the power generation of WTs, and it is necessary to describe the real wind distribution by a mathematical model. The two-parameter (k, c) Weibull distribution is widely accepted for the variable wind speed of a site, which can be formulated by Ref. [37]:

$$P_i^{dv}(V_i, k(\theta), C_i(\theta, x_i, y_i, V_i)) = \frac{k(\theta)}{C_i(\theta, x_i, y_i, V_i)} \left(\frac{V_i}{C_i(\theta, x_i, y_i, V_i)} \right)^{k(\theta)-1} e^{-\left(\frac{V_i}{C_i(\theta, x_i, y_i, V_i)} \right)^{k(\theta)}} \quad i \in V^{WT} \quad (1)$$

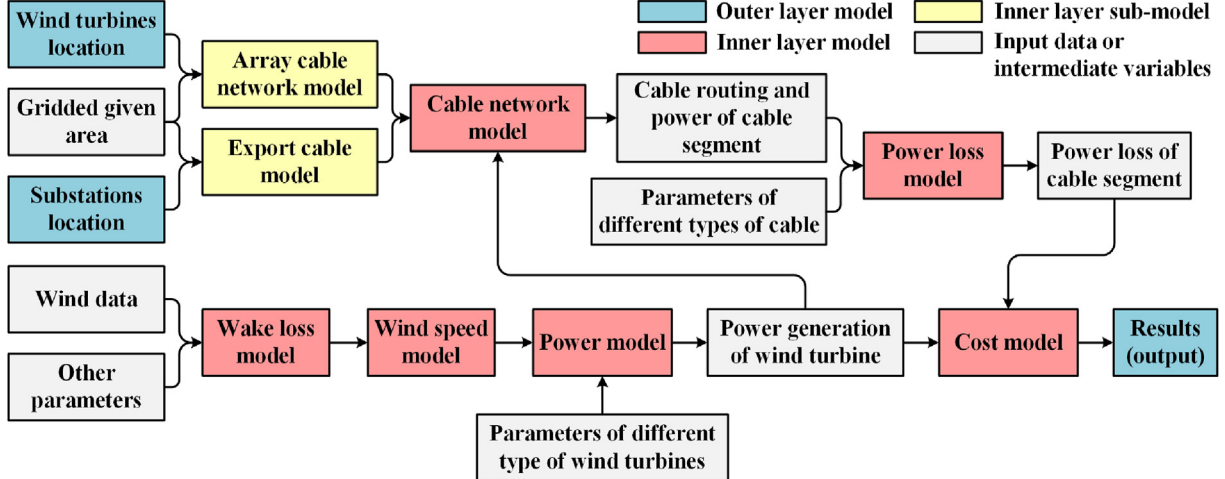


Fig. 1. The framework of the integrated model.

$$P_i^{cv}(V_i, k(\theta), C_i(\theta, x_i, y_i, V_i)) = 1 - e^{-\left(\frac{V_i}{C_i(\theta, x_i, y_i, V_i)}\right)^{k(\theta)}} \quad i \in V^{WT} \quad (2)$$

where P_i^{dv} is the probability density function, P_i^{cv} is the cumulative distribution function, $k(\theta)$ is the shape parameter. $k(\theta)$ is simulated by fitting the Weibull function based on the real data of wind speed and wind frequency, $C_i(\theta, x_i, y_i, V_i)$ is the scale parameter, which is a function of wind direction θ , the coordinates (x_i, y_i) and the wind speed V_i at the hub height of the WT.

2.3. Wake loss model

Wake loss is common in the power generation of multiple WTs. When wind flows through a WT, part of the kinetic energy will be transferred to the turbine blades. The wind speed will decrease in the downwind direction of the WT according to the law of conservation of energy. If there are other WTs in the wake region

where the wind speed decreases, the power output of these WTs will be reduced. In this research, multi-type wind turbines are taken into the consideration. Therefore, in addition to the relative position of the wind turbine on a 2D plane, the hub heights and rotation diameters of different wind turbines also become the important factors affecting the wake loss. Therefore, a 3D wake loss model is needed for the proposed problem.

A widely used wake loss model, the PARK model is applied in this study as shown in Fig. 2(a). It is assumed that the deficit of the wind speed expands linearly. The model is based on the Jensen theory which is firstly proposed by Jensen [6] and is improved by Katic et al. [46]. For the Weibull distribution wind distribution, it has been declared that the wake loss only affects $C_i(\theta, x_i, y_i)$ [2], which can be described as following [47]:

$$C_i(\theta, x_i, y_i, V_i) = c_i(\theta) \times (1 - V_i^{Def}) \quad i \in V^{WT} \quad (3)$$

where $c_i(\theta)$ can be determined by fitting the Weibull distribution based on the wind data of different wind directions, V_i^{Def} is the total wind speed deficit of i th WT and is calculated as follows [3]:

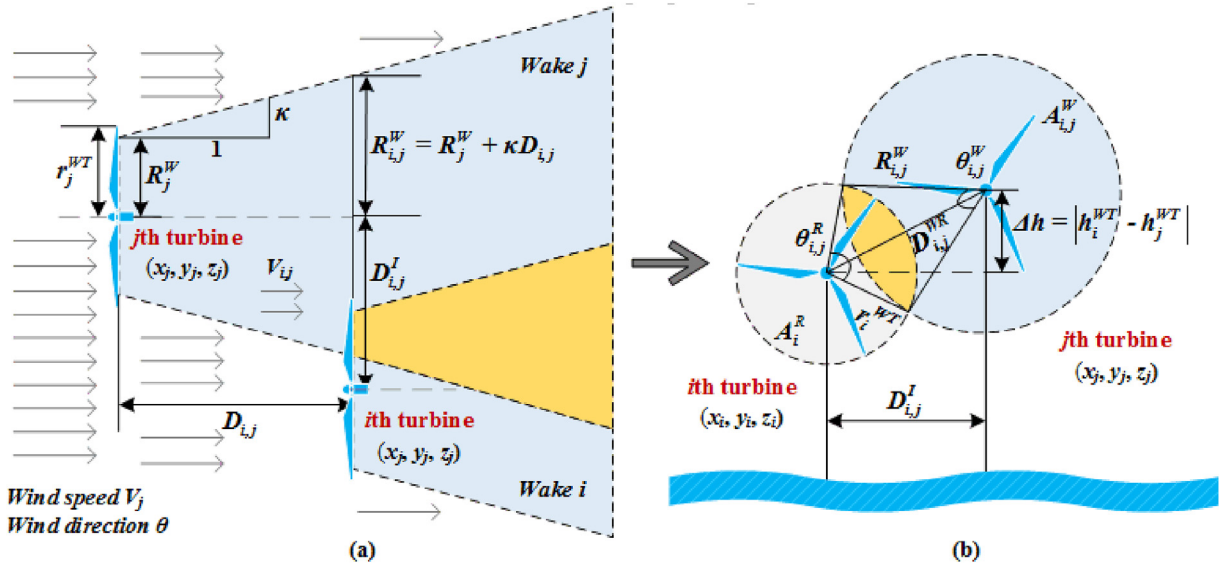


Fig. 2. (a) Jensen wake loss model and (b) Overlap area.

$$V_i^{Def} = \sqrt{\sum_{\substack{j=1 \\ j \neq i}}^{n^{WT}} \left(V_{ij}^{Def} \right)^2} \quad i, j \in V^{WT} \quad (4)$$

$$V_{ij}^{Def} = 1 - \frac{V_i}{V_{ij}} = \left(1 - \sqrt{1 - C_i^T} \right) \left(\frac{R_j^W}{R_j^W + \kappa_i D_{ij}} \right)^2 A_{ij}^{overlap} \quad i, j \in V^{WT} \quad (5)$$

$$R_i^W = r_i^{WT} \sqrt{\frac{1 + \sqrt{1 - C_i^T}}{2\sqrt{1 - C_i^T}}} \quad i \in V^{WT} \quad (6)$$

V_{ij}^{def} is the wind speed deficit caused by j th WT to i th WT, V_{ij} is the wind speed at i th WT after being affected by j th WT. κ_i indicates the wake spreading constant, D_{ij} is the distance between every two turbines following the wind direction θ . r_i^{WT} and C_i^T are the rotor radius and the thrust coefficient of the WT, R_j^W [48], is the downstream rotor radius. A_i^R is the rotor swept area of the downstream i th WT, $A_{ij}^{overlap}$ is the overlap area between A_i^R and the expanded wake area A_{ij}^W of the upstream WT, as shown in Fig. 2(b). $A_{ij}^{overlap}$ is calculated as follows [49]:

$$A_{ij}^{overlap} = \begin{cases} 0, & \text{if } R_{ij}^W + r_i^{WT} \leq D_{ij}^{WR} \\ \pi \left(r_i^{WT} \right)^2, & \text{if } R_{ij}^W - r_i^{WT} \geq D_{ij}^{WR} \\ \frac{1}{2} \left[\left(R_{ij}^W \right)^2 \left(\theta_{ij}^W - \sin \theta_{ij}^W \right) + \left(r_i^{WT} \right)^2 \left(\theta_{ij}^R - \sin \theta_{ij}^R \right) \right], & \text{otherwise} \end{cases} \quad i, j \in V^{WT} \quad (7)$$

$$R_{ij}^W = R_j^W + \kappa_i D_{ij} \quad i, j \in V^{WT} \quad (8)$$

$$\theta_{ij}^W = 2\cos^{-1} \left\{ \frac{\left(D_{ij}^{WR} \right)^2 + \left[\left(R_{ij}^W \right)^2 - \left(r_i^{WT} \right)^2 \right]}{2D_{ij}^{WR} R_{ij}^W} \right\} \quad i, j \in V^{WT} \quad (9)$$

$$\theta_{ij}^R = 2\cos^{-1} \left\{ \frac{\left(D_{ij}^{WR} \right)^2 - \left[\left(R_{ij}^W \right)^2 - \left(r_i^{WT} \right)^2 \right]}{2D_{ij}^{WR} r_i^{WT}} \right\} \quad i, j \in V^{WT} \quad (10)$$

$$D_{ij}^{WR} = \sqrt{(x_i - x_j)^2 + (y_i - y_j)^2 - D_{ij}^2 + (h_i^{WT} - h_j^{WT})^2} \quad i, j \in V^{WT} \quad (11)$$

D_{ij}^{WR} is the distance between the centers of the wake and turbine rotor which is shown in Fig. 2 (b). Other variables in Eq. (5) are calculated as follows:

$$V_i = v \left[\frac{\ln(h_i^{WT}/z_0)}{\ln(h/z_0)} \right] \quad i \in V^{WT} \quad (12)$$

$$\kappa_i = \frac{0.5}{\ln(h_i^{WT}/z_0)} \quad i \in V^{WT} \quad (13)$$

$$D_{ij} = \left| (x_i - x_j) \cos \theta + (y_i - y_j) \sin \theta \right| \quad i, j \in V^{WT} \quad (14)$$

$$C_i^T = \left(5.47581845 \times 10^{-6} V_i^{5.00641402} + 1.132584887 \right)^{-1} \quad i \in V^{WT} \quad (15)$$

where V_i [50] is the wind speed at h_i^{WT} which is the hub height of i th WT, z_0 is the surface roughness where the WT is located, v is the observed wind speed at h from wind data. The C_i^T curve is proposed

by Gualtieri [51] and is the best-fitting curve based on the real data provided by manufacturers for 50 onshore commercials WTs.

2.4. Power model

The selected model of power generation is classic and has been widely used in previous researches [33,52,53], which is described as follows [54].

$$P_i(V_i) = \begin{cases} 0, & V_i < v_i^{CI} \text{ or } V_i > v_i^{CO} \\ \frac{1}{2} \eta_i^{WT} \rho \pi \left(r_i^{WT} \right)^2 V_i^3, & v_i^{CI} \leq V_i < v_i^R \quad i \in V^{WT} \\ p_i^R, & v_i^R \leq V_i \leq v_i^{CO} \end{cases} \quad (16)$$

where η_i^{WT} and p_i^R are the power coefficient and rated capacity of the WT, respectively, ρ is the air density of the site. v_i^{CI} , v_i^R and v_i^{CO} are the cut-in speed, rated speed and cut-out speed of i th WT.

Combined the models of wind speed, wake loss and power, the power generation of i th WT, P_i is given by:

adding all the values of wind directions and wind speeds up as Eq. (18), where p_{d-1}^θ is the blowing probability of the $(d-1)$ th wind direction interval.

$$\begin{aligned}
 P_i &= \int_0^{2\pi} p^{d\theta}(\theta) d\theta \int_0^\infty P_i(V_i) P_i^{dv}(V_i, k(\theta), C_i(\theta, x_i, y_i, V_i)) dv \\
 &= \int_0^{2\pi} p^{d\theta}(\theta) d\theta \left\{ \begin{array}{l} \frac{1}{2} \eta_i^{WT} \rho \pi (r_i^{WT})^2 \int_{v^{CI}}^{v^R} V_i^3 \frac{k(\theta)}{C_i(\theta, x_i, y_i, V_i)} \left[\frac{V_i}{C_i(\theta, x_i, y_i, V_i)} \right]^{k(\theta)-1} e^{-\left[\frac{V_i}{C_i(\theta, x_i, y_i, V_i)} \right]^{k(\theta)}} dv \\ + p_i^R \int_{v^R}^{v^{CO}} \frac{k(\theta)}{C_i(\theta, x_i, y_i, V_i)} \left[\frac{V_i}{C_i(\theta, x_i, y_i, V_i)} \right]^{k(\theta)-1} e^{-\left[\frac{V_i}{C_i(\theta, x_i, y_i, V_i)} \right]^{k(\theta)}} dv \end{array} \right\} \\
 &= \int_0^{2\pi} p^{d\theta}(\theta) d\theta \left\{ \frac{1}{2} \eta_i^{WT} \rho \pi (r_i^{WT})^2 \int_{v^{CI}}^{v^R} V_i^3 d \left\{ 1 - e^{-\left[\frac{V_i}{C_i(\theta, x_i, y_i, V_i)} \right]^{k(\theta)}} \right\} + p_i^R \int_{v^R}^{v^{CO}} d \left\{ 1 - e^{-\left[\frac{V_i}{C_i(\theta, x_i, y_i, V_i)} \right]^{k(\theta)}} \right\} \right\}
 \end{aligned} \tag{17}$$

where $p^{d\theta}(\theta)$ is the probability density function of wind direction distribution. It is difficult to obtain the analytical solution of P_i and the wind characteristics that can be collected are discrete. Therefore, the integration can be approximated with the Riemann sum according to the discrete wind speed and wind direction. They can be discretized into $n^{Ve} + 1$ and $n^D + 1$ small bins ($V_s \in [v^{CI}, v^R]$ and $\theta_d \in [0, 2\pi]$) with equal width. P_i can be approximately expressed by

2.5. Cable network model

The 3D model of the cable network in this research is the inner layer of the proposed model, including two parts: (a) the cable network for the array cable from all the WTs to the offshore substation; (b) the cable routing for the export cable from the offshore substation to the onshore substation. The two parts are optimized

$$\begin{aligned}
 P_i &= \frac{1}{2} \eta_i^{WT} \rho \pi (r_i^{WT})^2 \sum_{s=1}^{n^{Ve}+1} \left(\frac{V_{s-1} + V_s}{2} \right)^3 \sum_{d=1}^{n^D+1} \left\{ (\theta_d - \theta_{d-1}) p_{d-1}^\theta \left\{ e^{-\left[\frac{V_{s-1}}{C_i\left(\frac{\theta_d+\theta_{d-1}}{2}, x_i, y_i, V_{s-1}\right)} \right]^{k\left(\frac{\theta_d+\theta_{d-1}}{2}\right)}} - e^{-\left[\frac{V_s}{C_i\left(\frac{\theta_d+\theta_{d-1}}{2}, x_i, y_i, V_s\right)} \right]^{k\left(\frac{\theta_d+\theta_{d-1}}{2}\right)}} \right\} \right\} \\
 &\quad + p_i^R \sum_{d=1}^{n^D+1} \left\{ (\theta_d - \theta_{d-1}) p_{d-1}^\theta \left\{ e^{-\left[\frac{v^R}{C_i\left(\frac{\theta_d+\theta_{d-1}}{2}, x_i, y_i, v^R\right)} \right]^{k\left(\frac{\theta_d+\theta_{d-1}}{2}\right)}} - e^{-\left[\frac{v^{CO}}{C_i\left(\frac{\theta_d+\theta_{d-1}}{2}, x_i, y_i, CO\right)} \right]^{k\left(\frac{\theta_d+\theta_{d-1}}{2}\right)}} \right\} \right\} \quad i \in V^{WT}; s \in S; d \in D
 \end{aligned} \tag{18}$$

independently in the two areas (array cable area and export cable area) of the wind farm which are separated by the offshore substation.

2.5.1. Array cable network

A three steps method is applied for the array cable network.

- (1). A linear programming (LP) model is established to optimize the submarine cable laying route on the gridded array cable area with the shortest length between each two WTs or one WT and the offshore substation.
- (2). The minimum spanning tree $T(V^T, E^T, W^T)$ is generated according to the connected graph $G(V^C, E^C, W^C)$, where V^C includes all the WTs and the offshore substation, W^C reflects the 3D length optimized by step (1), and Kruskal algorithm is applied in this section.
- (3). The power transmitted by each submarine cable segment is calculated by an LP model based on $T(V^T, E^T, W^T)$.

The LP model in step (1) is established based on the gridded site of the array cable area which can be described by an initial graph $G(V^{AC}, E^{AC}, W^{AC})$ of the gridded array cable area. It is described as follows:

$$\min \quad obj_{1,u,v} = \sum_{i=1}^{n^{VAC}} \sum_{j=1}^{n^{VAC}} l_{i,j} P_{u,v,i,j}^R \quad i,j \in V^{AC}; u,v \in V^C \quad (19)$$

$$\text{s.t. } \sum_{i=1}^{n^{VAC}} \sum_{j=1}^{n^{VAC}} P_{u,v,i,j}^R - \sum_{i=1}^{n^{VAC}} \sum_{j=1}^{n^{VAC}} P_{u,v,j,i}^R = p_{u,v,i}^R \quad i,j \in V^{AC}; u,v \in V^C \quad (20)$$

$$l_{i,j} = \sqrt{(x_i - x_j)^2 + (y_i - y_j)^2 + (z_i - z_j)^2} \quad i,j \in V(V^{AC} \cup V^{EC}) \quad (21)$$

$$z_i = \begin{cases} z_i^0, & \text{if } b_i = 0 \\ z^M, & \text{otherwise} \end{cases} \quad i \in V \quad (22)$$

The objective function is minimizing the sum of the submarine cable length multiplied by the power on cable segments. n^V is the number of vertexes in V^{AC} . Eq. (20) is the constraint on the energy balance of each vertex in the area grid. Different from the 2D model, the length between every two vertexes $l_{i,j}$ is calculated according to the 3D distance in space based on the seabed topography data. Besides, the elevations of obstacle areas are marked by z^M in Eq. (22). Eq. (22) displays that if the i th vertex is an obstacle, z_i will equal to z^M which is a sufficiently small negative constant to avoid the submarine cable passing through this vertex.

According to Eqs. (21) and (22), the difference between the obstacle area and the normal area is in the elevation, and the obstacle-avoiding is achieved by the optimization of the 3D length of the cable. Therefore, if the model does not consider the elevation and becomes a 2D model, the obstacle-avoiding scheme cannot be obtained.

$$B_{u,v,i,j}^{AC} = \begin{cases} 1, & \text{if } P_{u,v,i,j}^R > 0 \\ 0, & \text{otherwise} \end{cases} \quad i,j \in V^{AC}; u,v \in V^C \quad (23)$$

$$W_e^C(u,v) = W_{u,v}^C = \sum_{i=1}^{n^{VAC}} \sum_{j=1}^{n^{VAC}} l_{i,j} B_{u,v,i,j}^{AC} \quad i,j \in V^{AC}; u,v \in V^C \quad (24)$$

Based on the solution of the above LP model, the weight $W_{u,v}^C \subseteq W^C$ is obtained by Eq. (24) and the graph $G(V^C, E^C, W^C)$ can be generated. According to graph G , the minimum spanning tree can be found, which is the connected weighted undirected subgraph $T(V^T, E^T, W^T)$ with the smallest weight.

$$\min \quad obj_2 = \sum_{e=1}^{n^{TE}} W_e^T(u,v) \quad u,v \in V^C; e \in E^C \quad (25)$$

$$n^{TE} = |V^C| - 1 \quad (26)$$

$$W_{u,v}^T = W_{v,u}^T \quad (27)$$

Then the power on each edge (cable segment) of the minimum spanning tree $T(V^T, E^T, W^T)$ is calculated by the following LP model.

$$\min \quad obj_3 = \sum_{u=1}^{n^{VT}} \sum_{v=1}^{n^{VT}} W_{u,v}^T P_{u,v}^R \quad u,v \in V^T \quad (28)$$

$$\text{s.t. } \sum_{u=1}^{n^{VT}} \sum_{v=1}^{n^{VT}} P_{u,v}^R - \sum_{u=1}^{n^{VT}} \sum_{v=1}^{n^{VT}} P_{v,u}^R = p_u^R \quad u,v \in V^T \quad (29)$$

2.5.2. Export cable routing

The model of the export cable routing between the offshore substation and the onshore substation is similar to Eqs. 19–24 for the array cable.

$$\min \quad obj_{1,u,v} = \sum_{i=1}^{n^{VEC}} \sum_{j=1}^{n^{VEC}} l_{i,j} P_{u,v,i,j}^R \quad i,j \in V^{EC}; u,v \in V^R \quad (30)$$

$$\text{s.t. } \sum_{i=1}^{n^{VEC}} \sum_{j=1}^{n^{VEC}} P_{u,v,i,j}^R - \sum_{i=1}^{n^{VEC}} \sum_{j=1}^{n^{VEC}} P_{u,v,j,i}^R = p_{u,v,i}^R \quad i,j \in V^{EC}; u,v \in V^R \quad (31)$$

$$B_{u,v,i,j}^{EC} = \begin{cases} 1, & \text{if } P_{u,v,i,j}^R > 0 \\ 0, & \text{otherwise} \end{cases} \quad i,j \in V^{EC}; u,v \in V^R \quad (32)$$

$$W_e^R(u,v) = W_{u,v}^R = \sum_{i=1}^{n^{VEC}} \sum_{j=1}^{n^{VEC}} l_{i,j} B_{u,v,i,j}^{EC} \quad i,j \in V^{EC}; u,v \in V^R \quad (33)$$

Put the results of the two types of cable networks together, the final cable network is given by:

$$T(V^A, E^A, W^A) = T(V^T, E^T, W^T) \cup T(V^R, E^R, W^R) \quad (34)$$

2.6. Power loss model

The energy loss calculation is usually based on annual average full-load hours, which can be expressed as [55,56]:

$$P_{ij}^{loss} = 3 \left(I_{ij}^R \right)^2 N_{ij}^C (1 + \lambda_{1,p} + \lambda_{2,p}) r_p^{ES} W_{ij}^A H^F \quad i,j \in V^A; p \in P \quad (35)$$

where I_{ij}^R is the rated current denoted as the sum of currents produced by WTs and pass-through this cable segment to the substation. $\lambda_{1,p}$ and $\lambda_{2,p}$ are the sheath loss factor and armor loss factor for p th type of cable, r_p^{ES} is the conductor resistance of p th type of cable, H^F is the annual average full-load hours. A feasible cable connecting every two vertexes must not be over the current limit of type p cable as shown in Eq. (36).

$$I_{ij}^R \leq i_p^R \quad i,j \in V^A; p \in P \quad (36)$$

Three-core SL type cable is used in this study, so Eq. (37) takes the following form [57]:

$$I_{ij}^R = \frac{P_{ij}^R}{\sqrt{3} \cos \varphi u_p^R N_{ij}^C} \quad i,j \in V^A; p \in P \quad (37)$$

where P_{ij}^R is the power in a cable segment when all the WTs are at rated power output, $\cos \varphi$ is the power factor and u_p^R is the rated voltage of the type p cable, N_{ij}^C is the cable number between node i and node j . The cross-section of each cable segment is selected according to the calculated rated current. Simultaneously, its r_p^{ES} and inductive reactance r_p^{EA} are determined as well.

$$\lambda_{1,p} = \frac{r^S}{r_p^{ES}} \frac{1}{1 + \left(\frac{r^S}{r_p^{EA}} \right)^2} \quad p \in P \quad (38)$$

$$\lambda_{2,p} = 1.23 \frac{r^A}{r_p^{ES}} \left(\frac{2c_p^D}{d^A} \right)^2 \frac{1}{1 + \left(\frac{2.77r^A 10^6}{\omega} \right)^2} \left(1 - \frac{r_p^{ES}}{r^S} \lambda_{1,p} \right) \quad p \in P \quad (39)$$

$$c_p^D = d_p^{CS} + 70 \quad p \in P \quad (40)$$

$$\omega = 2\pi f \quad (41)$$

$$H^F = \frac{8760 \sum_{i=1}^{n^{WT}} P_i}{\sum_{i=1}^{n^{WT}} P_i^R} \quad i,j \in V^{WT} \quad (42)$$

where r^S is the resistance of sheath or screen per unit length of cable at its maximum operating temperature, r_p^{EA} is the reactance per unit length of sheath or screen per unit length of cable, r^A is the resistance of armor at maximum armor temperature, c_p^D is the distance between the axis of a conductor and the cable center, d^A is the mean diameter of armor, ω is the angular frequency, f is the frequency.

2.7. Cost model

2.7.1. Objective function

The objective function of the outer layer method is maximizing

the annual economic benefit (B^{NI}) which is given by:

$$\max \quad obj = B^{NI} = B^{EP} - (C^{energy} + C^{loss} + C^{cable}) \quad (43)$$

$$\begin{aligned} & \left\{ \begin{array}{l} 1 \leq (N_i^{WT} \wedge N^{OFS}) \leq n^{AC} \\ 1 \leq N^{ONS} \leq n^{ERMax} \\ n^{ARMin} \leq N^{Row} \leq n^{ARMax} \\ n^{ACMin} \leq N^{Col} \leq n^{ACMax} \\ (x_i - x_j)^2 + (y_i - y_j)^2 \geq (4 \times 2r_i^{WT})^2 \end{array} \right. \quad i,j \in V^{WT} \end{aligned} \quad (44)$$

where B^{EP} is the annual electricity production benefit, C^{energy} is the cost of energy, C^{loss} is the cost of energy loss and C^{cable} is the cost of cables. The last constraint is the distance constraints [58] between each two WTs to reduce interaction. Any two WTs which are located at (x_i, y_i, z_i) and (x_j, y_j, z_j) should satisfy the constrain. Other constraints limit the locations of WTs, offshore (onshore) substations and the array cable area in their respective specific gridded areas.

2.7.2. Costs

The benefit and costs are calculated as follows:

$$B^{EP} = 8760 c^E \sum_{i=1}^{n^{WT}} P_i \quad i \in V^{WT} \quad (45)$$

$$C^{energy} = \frac{r^{IT} \left(\sum_{i=1}^{n^{WT}} c_i^{WT} + \text{floor} \left(\frac{n^{WT}}{n^{OFS}} \right) c^{OFS} + c^{ONS} \right) \times es + n^{WT} c^{OM}}{1 - (1 + r^{IT})^{-n^Y}} \quad i \in V^{WT} \quad (46)$$

$$es = \left(\frac{2}{3} + \frac{1}{3} e^{-0.00174(n^{WT})^2} \right) \quad (47)$$

$$C^{loss} = \sum_{m=1}^{n^Y} \sum_{i=1}^{n^{VA}} \sum_{j=1}^{n^{VA}} \frac{c^E}{(1 + r^{IF})^m} P_{ij}^{loss} \quad i,j(i \neq j) \in V^A; m \in Y \quad (48)$$

$$C^{cable} = \frac{r^{IT} \left(\sum_{i=1}^{n^{VA}} \sum_{j=1}^{n^{VA}} W_{ij}^A (c_p^C + c^T) + \sum_{w=1}^{n^{WT}} |z_w| c_p^C \right)}{1 - (1 + r^{IT})^{-n^Y}} \quad i,j(i \neq j) \in V^A; w \in V^{WT}; p \in P \quad (49)$$

where C^{energy} [58,59] is the cost of the power generation, c^E is electricity price, c^{OM} is operation & maintenance cost, es is the economies of scale defined in Ref. [58]. c_p^C is the unit price of type p cable, c^T is the cost of trench construction [57], r^{IF} is the inflation rate, r^{IT} is the interest rate, n^{OFS} is the number of the offshore substation, n^Y is the wind farm lifetime. c_i^{WT} , c^{OFS} and c^{ONS} are the costs of the WT, offshore substation and onshore substation. They are calculated as follows [17].

$$c_i^{WT} = 1.6 P_i^R - 1.9 \quad i \in V^{WT} \quad (50)$$

$$c^{OFS} = 0.11 \sum_{i=1}^{n^{WT}} P_i^R \quad i \in V^{WT} \quad (51)$$

$$c^{ONS} = \frac{c^{OFS}}{2} \quad (52)$$

3. Algorithms

Compared with traditional algorithms, meta-heuristic algorithms are more efficient than blind search algorithms and can obtain relatively better solutions in a limited time. Therefore, these algorithms have been widely applied in wind farm optimization. GA is popular in various optimization problems due to its good performance of global search and strong robustness. It starts with a set of an initial solution called chromosomes which are composed of genes (variables). The population evolves through a series of operations including selection (tournament selection in the proposed algorithm), crossover (single point) and mutation. In the process, good individuals are retained and can reproduce offspring, while bad individuals are eliminated and regenerated randomly. ACO was initially proposed by Dorigo and co-workers [60], it was formulated for combinatorial optimization problems [61]. It is apt at finding the optimal solution based on a given nearby initial solution. In each iteration, each ant probabilistically constructs a path (roulette wheel selection in the proposed algorithm) that depends on the pheromone concentration. A path with edges is equivalent to a

solution composed of variables. Then the paths found by the different ants are compared and the pheromone concentration will be updated. The edge with higher pheromone concentration tends to be selected by more ants.

Due to the nonlinear power curves, wake model, the distance constraint for discrete variables of WTs locations and the model of 3D obstacle-avoiding cable routing, the integrated model has strong non-convexity. The model coupling integer nonlinear programming (INLP, outer layer) and LP (inner layer) is a complex MINLP model. It is difficult to find the best solution powerfully in a feasible time even with meta-heuristic algorithms. Therefore, one aim of the work is to improve the effectiveness of the traditional meta-heuristic algorithm to make it more suitable for solving the proposed problem. GA and ACO are combined to solve the proposed model and the framework of the proposed algorithm is shown in Fig. 3.

The initialization performance directly affects the quality of the optimal solution found by ACO. In this work, the solution found by GA is used as the feasible initial solution for IACO. On the other hand, the evolution of variables in IACO needs to conform to the characteristics of the proposed problem. In this study, variables representing relative positions of WTs for a reasonable layout may follow some rules. For example, affected by the wind direction, WTs may tend to be distributed along the wind direction to maximize the use of wind resources. These variables do not affect the objective function individually, it is necessary to preserve the characteristics of the good solution as much as possible. Thus, the new solution is generated by operating on a small number (two in this study) of randomly selected variables instead of all variables,

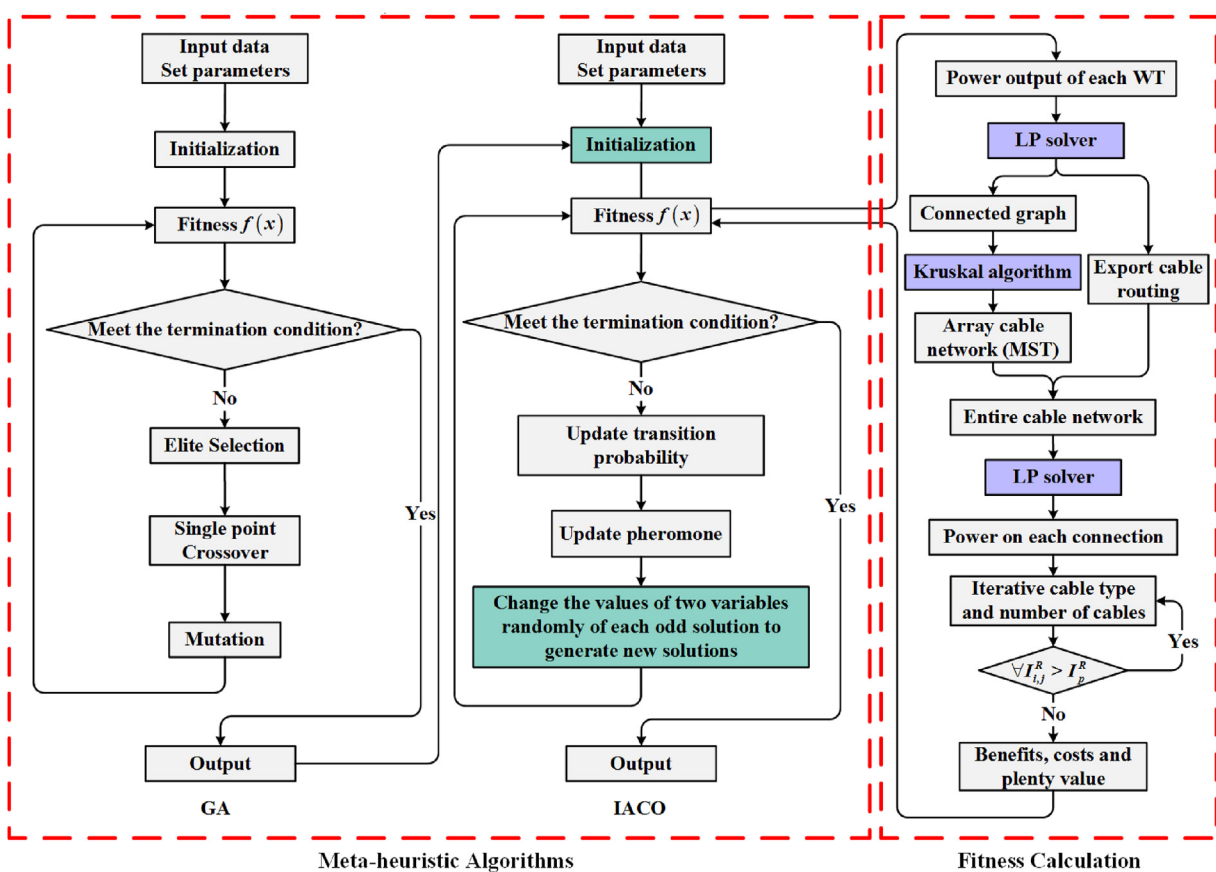


Fig. 3. The framework of the hybrid algorithm.

Table 1
Scenario summary.

	Algorithm	Objective function	Dimension	WT type	Site selection
Scenario 1.1	ACO based	B^{NI}	3D	Single	Optimize
Scenario 1.2	GA based	B^{NI}	3D	Single	Optimize
Scenario 1.3	GA-ACO based	B^{NI}	3D	Single	Optimize
Scenario 1.4	GA-IACO based	B^{NI}	3D	Single	Optimize
Scenario 2	The best	$B^{EP} - C^{energy}$	3D	Single	Optimize
Scenario 3	The best	$B^{EP} - (C^{energy} + C^{cable})$	3D	Single	Optimize
Scenario 4	The best	B^{NI}	2D	Single	Optimize
Scenario 5	The best	B^{NI}	3D	Multiple	Fix
Scenario 6	The best	B^{NI}	3D	Multiple	Optimize
Sensitivity analysis	The best	B^{NI}	3D	Multiple	Optimize

which not only retains the main characteristics of the current best solution more directly but also retains a certain search space.

To get solutions that satisfy distance constraints in inequality (44) of the outer layer model, a penalty function $B^{PV}(X)$ is used to exclude the solutions that cannot meet the constraints in the evolution. It is given by:

$$f(X) = obj(X) - B^{PV}(X) \quad (53)$$

$$B^{PV}(X) = \delta \sum_{i=1}^{n^{WT}} \sum_{j=1}^{n^{WT}} B_{ij} \quad i, j \in V^{WT} \quad (54)$$

$$B_{ij} = \begin{cases} 1, & \text{if } (x_i - x_j)^2 + (y_i - y_j)^2 < (4 \times 2r_i^{WT})^2 \\ 0, & \text{otherwise} \end{cases} \quad i, j \in V^{WT} \quad (55)$$

X represents a set of decision variables of the model, i.e. a potential solution. $f(X)$ is the fitness function and $obj(X)$ is the objective function. δ is the plenty factor (a sufficiently large positive constant). Other constraints in the model are implemented by specifying the upper and lower bounds of the variable in the meta-heuristic algorithms.

The inner layer algorithm includes an LP solver in Matlab for LP models and the Kruskal algorithm for the MST problem. For the LP solver, the dual-simplex method is applied. Kruskal algorithm is a classic heuristic algorithm for solving the problem of MST, it is based on the greedy algorithm and the pseudocode can be expressed as below.

Kruskal algorithm $[G(V, E, W)]$

```

 $T \leftarrow \emptyset$ 
for each vertex  $v \in V$  do
     $T = T \cup \{v\}$ 
Sort all the edges in  $E$  by the weights in  $W$ 
for each edge  $e(u, v) \in E$  do
    if  $u$  and  $v$  are not in the same subtree then
         $T = T \cup \{(u, v)\}$ 
    Merge the subtrees of  $u$  and  $v$ 
return  $T$ 

```

Based on the results of the entire cable network optimized by the inner layer algorithms, the type and number of cables on each edge will be obtained. For each edge, the current rate under different types of cables will be calculated in turn. In this process, if the current of the p th type of cable is less than its current carrying capacity, the cable is feasible. If all the types of cable are not

feasible, the cable number on the edge will be increased until there is at least one type of cable that meets the current limit.

4. Case study

4.1. Scenarios description

To illustrate the effectiveness and feasibility of the proposed method, a case study is established based on the available public data of a representative offshore wind farm named skipjack wind farm. It consists of four comparative experiments and one sensitivity analysis. First, algorithm comparison is done to illustrate the advantage of the developed algorithm GA-IACO. Second, the optimizations with different objective functions are achieved to verify the necessity of the proposed model. Third, the optimizations of different spatial dimensions are compared, and the difference between the results of 3D and 2D is discussed. Then, different types of WTs are taken into the consideration, as well as the site optimization of the array cable area. At last, in the case of the same total rated capacity, a sensitivity analysis is carried out on the proportion of the number of different WTs, and the influence of it on the total revenue of the offshore wind farm. The specific conditions of different scenarios are listed in Table 1. Additionally, the optimization is implemented by Matlab in Windows 10. The CPU is Intel(R) Core (TM) i7-8700 CPU @ 3.2 GHz 3.19 GHz.

4.2. Data collection and preprocessing

4.2.1. Wind farm and WT

The skipjack wind farm is built on the outer continental shelf offshore Delaware in the United States, approximately 31 km from the coast opposite Fenwick Island [62]. At a modest scale, Skipjack Wind is the right size project for Delmarva as it enters America's growing offshore wind industry. It will come online second half of 2026 and is a representative wind farm. The rated power of the windfarm is 120 MW and the type of WTs is Haliade-X. To illustrate the proposed model that can handle the optimization with multi-type WTs, Haliade 150 is added to the case study. The parameters

Table 2
WT parameters.

	Haliade-X	Haliade 150
Rated capacity (MW)	12	6
Cut-in wind speed (m/s)	3.5	3
Rated wind speed (m/s)	11	12
Cut-out wind speed (m/s)	28	25
Hub height (m)	135	100
Rotor diameter (m)	109.1	75.4
Frequency (Hz)	50	50

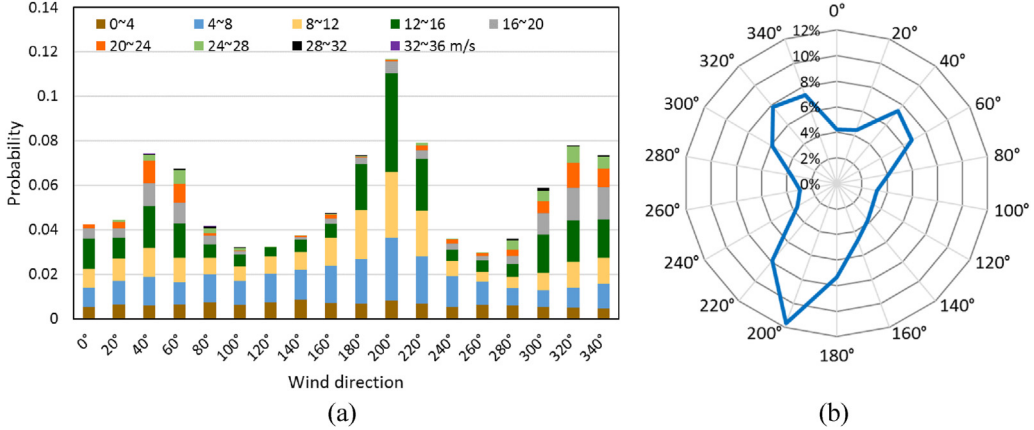


Fig. 4. (a) The original wind speed distribution and (b) Wind rose diagram.

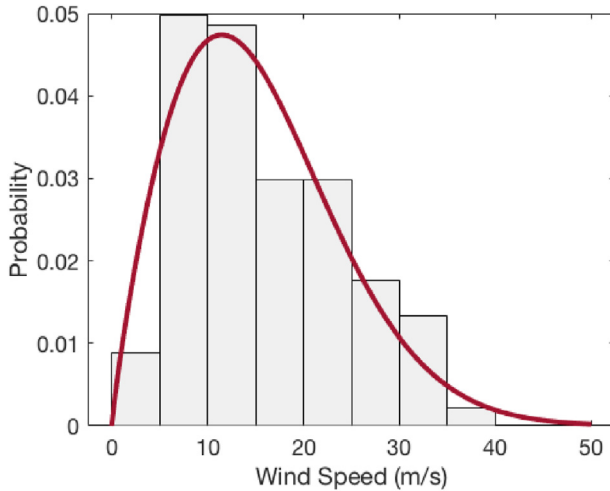


Fig. 5. Weibull distribution (Haliade-X, $\theta = 10^\circ$).

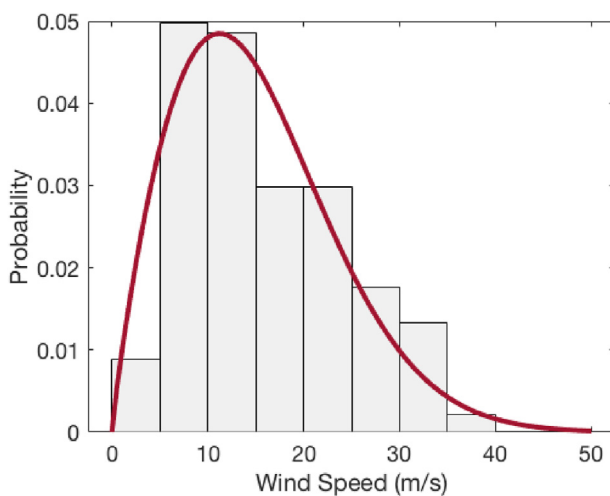


Fig. 6. Weibull distribution (Haliade 150, $\theta = 10^\circ$).

of WTs are shown in **Table 2**. Due to insufficient official data, the rated wind speed of Haliade-X is assumed.

4.2.2. Wind data

The wind data (see Fig. 4) is collected from the official website of

Table 3
The preprocessed wind data summary.

k	c (Haliade-X)	c (Haliade 150)	θ_{d-1}	θ_d	P_{d-1}^θ
2.27	18.62	18.21	0	20	0.0422
1.86	17.32	16.94	20	40	0.0445
2.13	21.19	20.72	40	60	0.0742
2.12	23.10	22.58	60	80	0.0675
1.52	17.98	17.58	80	100	0.0415
1.75	16.53	16.16	100	120	0.0319
1.92	13.02	12.73	120	140	0.0326
1.95	13.10	12.81	140	160	0.0375
1.87	14.75	14.42	160	180	0.0471
2.17	15.53	15.18	180	200	0.0734
2.71	17.35	16.96	200	220	0.1167
2.37	17.41	17.02	220	240	0.0790
1.94	15.65	15.30	240	260	0.0361
1.85	14.75	14.42	260	280	0.0295
1.53	18.65	18.23	280	300	0.0361
2.12	23.49	22.96	300	320	0.0587
2.46	25.02	24.46	320	340	0.0779
2.35	24.51	23.96	340	360	0.0735

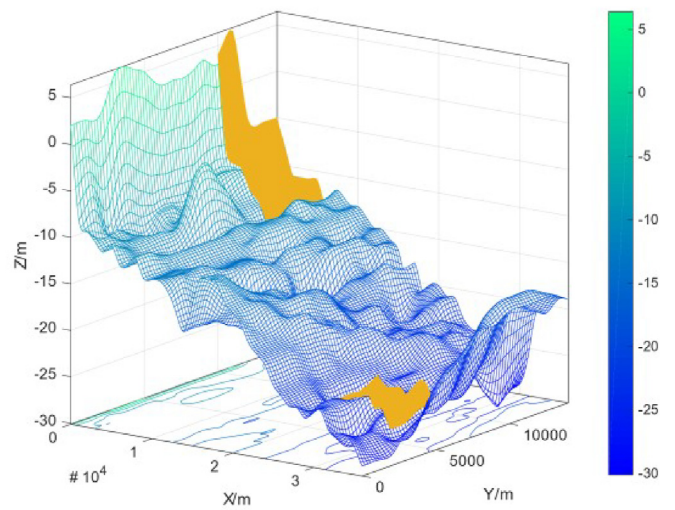


Fig. 7. The preprocessed seabed terrain (3D).

National Centers for Environmental Information (NOAA) [63]. The original data were collected every hour for a year in Delaware bay of the United States.

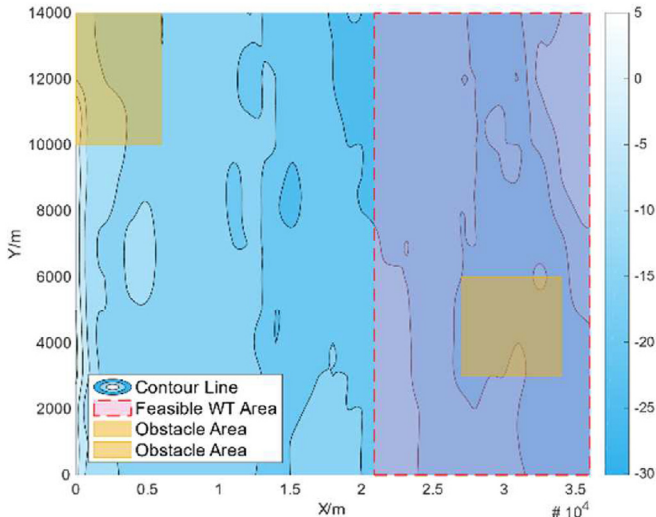


Fig. 8. The preprocessed seabed terrain (2D).

Table 4
XLPE submarine cable parameters.

Type	Conductor Cross-section(mm^2)	c_p^E (k\$/km)	r_p^{ES} (Ω/km)	Inductance (mH/km)	u_p^R (kV)	i_p^R (A)	d_p^{CS} (mm)
1	95	47.88	0.310	0.44	66	300	32.9
2	120	60.04	0.245	0.43	66	340	34.4
3	150	62.10	0.196	0.41	66	375	36.0
4	185	67.31	0.159	0.40	66	420	37.6
5	240	77.76	0.123	0.38	66	480	40.1
6	300	100.87	0.098	0.37	66	530	42.4
7	400	120.38	0.074	0.35	66	590	45.3
8	500	142.00	0.059	0.34	66	655	48.9
9	630	196.72	0.047	0.33	66	715	52.6
10	800	237.82	0.037	0.32	66	775	56.6
11	1000	275.38	0.030	0.31	66	825	61.6
12	500	283.99	0.059	0.43	220	655	80.5
13	630	393.44	0.047	0.41	220	715	82.2
14	800	475.64	0.037	0.4	220	775	86.2
15	1000	550.76	0.030	0.38	220	825	90.4

Table 5
Other parameters of the model summary.

Parameter	Value	Parameter	Value	Parameter	Value
c^E (\$/kWh)	0.117	f (Hz)	50	r^{IT}	3%
c^{OM} (\$/year)	15,210	h (m)	1.5	z_0 (m)	0.0002
c^T (\$/km)	2077.12	n^Y (year)	25	ρ (kg/m ³)	1.225
d^A (mm)	4.5–5	r^{IF}	5%	$\cos \varphi$	0.75

Table 6
The results of comparative experiments.

(\$/a)	B^{EP} (10^7)	C_{energy} (10^7)	C^{loss} (10^5)	C^{cable} (10^6)	B^{PV}	Fitness (10^7)
Scenario 1.1	4.0767	1.9974	1.2689	5.1666	0	1.5499
Scenario 1.2	4.0648	1.9974	1.5478	5.0742	0	1.5445
Scenario 1.3	4.0808	1.9974	1.3186	5.2403	0	1.5462
Scenario 1.4	4.0756	1.9974	1.9847	4.6974	0	1.5886
Scenario 2	4.1116	1.9974	2.7028	6.1448	0	1.4727
Scenario 3	4.0979	1.9974	1.8332	5.2990	0	1.5523
Scenario 4	4.0578	1.9974	2.0577	4.7752	0	1.5622
Scenario 5	4.0380	2.0979	1.5490	5.3741	0	1.3872
Scenario 6	4.0672	2.0979	1.1571	5.6285	0	1.3949

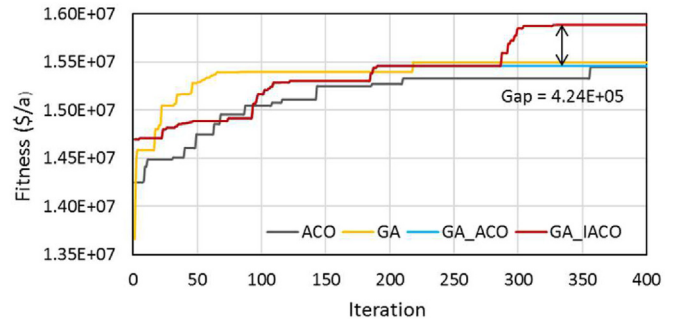


Fig. 9. Fitness iterations of different algorithm.

The preprocessing of the wind data includes fitting all the wind speeds in each wind direction interval and probability statistics for all wind directions. Note that the wind speed at different heights is considered in the proposed model. Therefore, for different types of WTs, fitting results of the Weibull distribution are slightly different in the same direction, as shown in Figs. 5 and 6.

All the preprocessed results are shown in Table 3.

4.2.3. Gridded bathymetry data

The boundary of the study area is assumed as 38.5–38.6°N, 74.73–75.06°W. The gridded bathymetry data of this sea area is collected from the General Bathymetric Chart of the Oceans (GEBCO) [64]. In this study, data preprocessing is conducted by Python with the GDAL library. First, the original GeoTiff data is processed by the GDAL library to acquire the affine georeferencing transform information and the elevation matrix. With the acquired transform information and matrix, the defined area polygon is divided into 1896 vector grids under the geographic coordinate system. On the other hand, we sampled 12,993 points with an interval of 200 m in both longitude and latitude within the predefined area rectangle boundary. In fact, meshing has a great influence on the solution speed and solution quality. In practical applications, the division of the grid size needs to be adjusted and verified according to different cases. With the vector grids and points, an overlapping analysis is conducted to match the related grids and points to get the elevation of each sampling point. To reduce the computation time of the distance between sampling points, we project all sampling points to the geodetic coordinate system and translate all points so that the lower-left point is overlapped with the origin.

After we get the preprocessed gridded data, the obstacle (restricted) area, where WTs and cables are prohibited is added to generate the final given area of the optimization. The size and locations of obstacle areas are assumed. The obstacle shape is assumed as rectangular. The method proposed in this research can be applied to optimization considering obstacle areas with

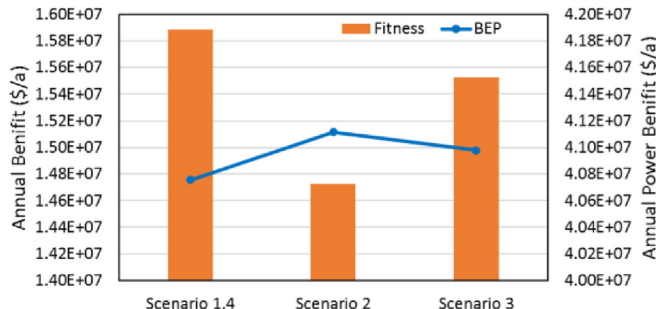


Fig. 10. The results of annual benefit and fitness.

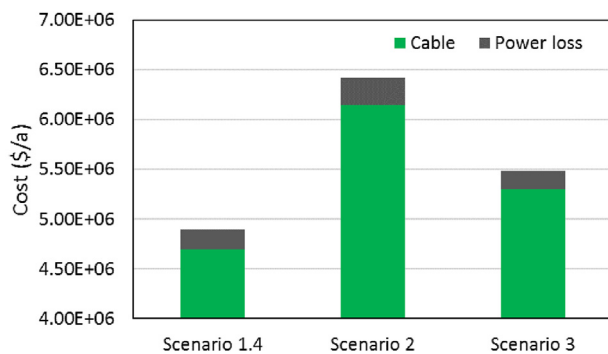


Fig. 11. The results of costs (Scenarios 1.4,2,3).

irregular shapes. The processed gridded area is shown in Figs. 7 and 8. The feasible WT area ($15 \text{ km} \times 14 \text{ km}$) in Fig. 8 is for the site selection of the cable (or WT) array area ($8 \text{ km} \times 8 \text{ km}$).

4.2.4. Submarine cable data

Generally, the voltage of array cables is different from that of the export cable. 66 kV and 220 kV submarine cables are used for array cable and export cable, respectively. The type of three-core SL XLPE cable is selected in this section and the parameters are listed in Table 4.

4.2.5. Other parameters

Table 5 shows the parameters required by the proposed model except for the above data.

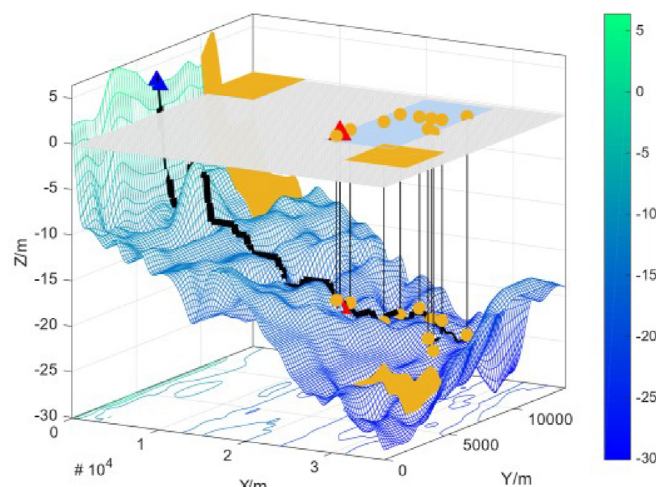


Fig. 12. 3D layout of Scenario 1.4.

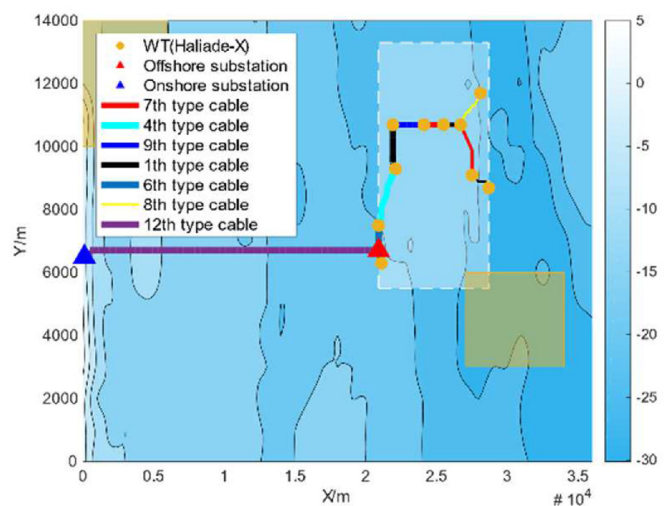


Fig. 13. 2D layout of Scenario 1.4.

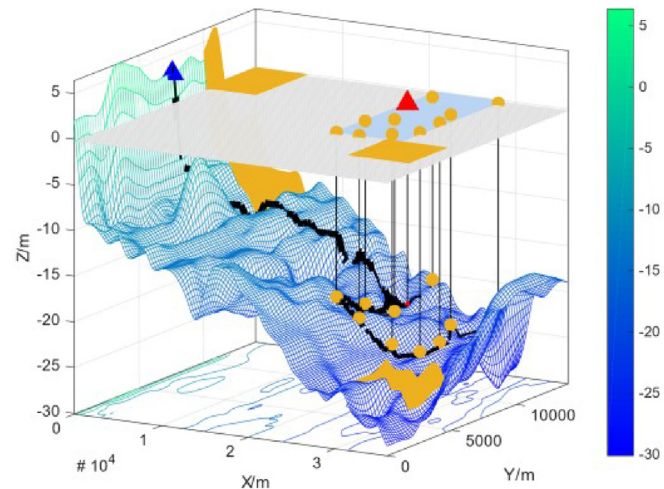


Fig. 14. 3D layout of Scenario 2.

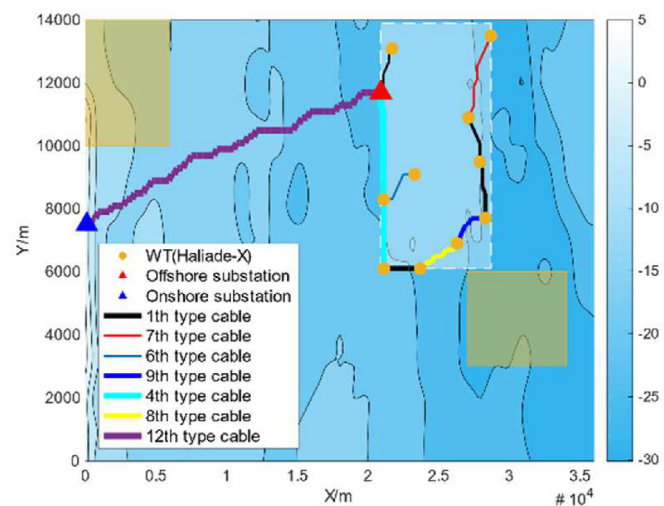


Fig. 15. 2D layout of Scenario 2.

5. Results and discussion

The overall results of the comparative experiments are shown in Table 6. All penalty values are 0, indicating that the optimization in all scenarios has converged, that is, all variables have met the constraints. The energy costs of scenarios 1–6 are equal because these scenarios have the same total rated output power and all the WTs are the same type.

5.1. Algorithm comparison

The optimizations by traditional GA, ACO, GA-ACO and the proposed hybrid algorithm (GA-IACO) are compared in this section. GA-ACO means that the initial solution of ACO is from the optimal solution by GA, which is the same as GA-IACO. The difference between GA-ACO and GA-IACO is the methods of solution generation in every iteration. As shown in Fig. 9, the fitness optimized by GA, ACO and GA-ACO are similar, while GA-IACO has the best performance. Specifically, the result of Scenario 1.4 is about 2.6% more than scenarios 1.1 and 1.2, which illustrates the necessity of the combination of GA and IACO, as well as the significance of the determination of the initial solution for IACO. After 200 iterations by GA, the fitness of Scenario 1.4 sees several obvious climbs, while the solution of Scenario 1.3 does not change. This proves that the evolutionary operation of IACO is more efficient than ACO. It can be concluded that GA-IACO conforms to the characteristics of the integrated model proposed in this study and is more powerful.

5.2. Objective function comparison

The comparison of the different objective functions is achieved to illustrate the advantages of the proposed synchronous model. Scenario 1.4, which considers issues such as power generation, cable cost and energy loss, obtains the most annual benefit with 15.89 million dollars. Almost a 7.87% increase is observed compared with Scenario 2 which only takes power generation into account. The specific results are shown in Figs. 10 and 11 intuitively. From Fig. 10, Scenario 2 has the highest benefit of power production, but its fitness is the lowest. The situation of Scenario 1.4 is the opposite, indicating that the cable routing and energy loss should not be ignored in the optimization. Energy loss cost is not taken into consideration in Scenario 3, resulting in a 2.29% decrease in the annual benefit compared with Scenario 1.4. The difference between the results of these two scenarios is smaller because energy loss

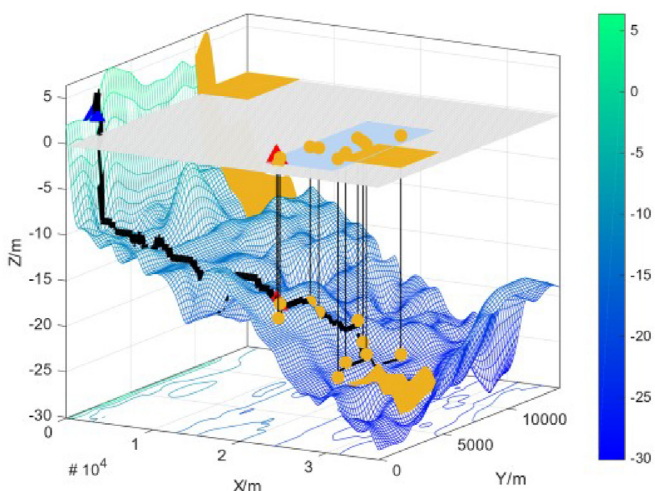


Fig. 16. 3D layout of Scenario 4.

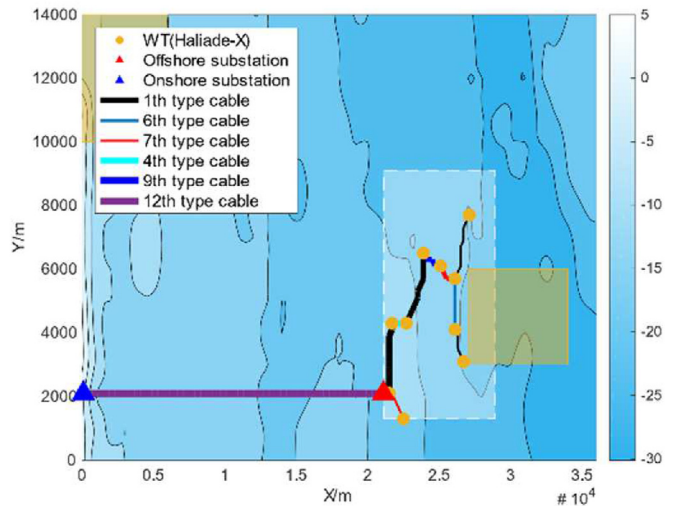


Fig. 17. 2D layout of Scenario 4.

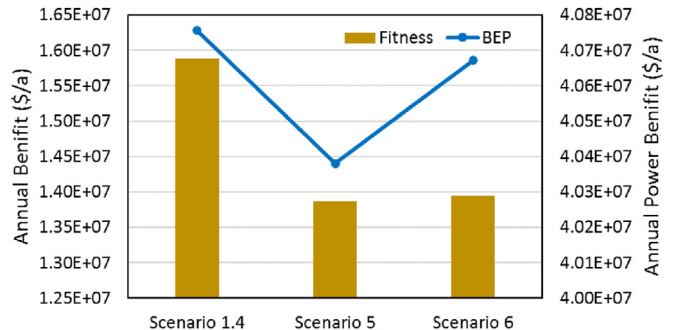


Fig. 18. The results of annual benefit and fitness.

cost accounts for a much smaller proportion of the total cost, as shown in Fig. 11. This section proves that a better layout of the offshore wind farm can be obtained by solving the proposed model than the one considering only power generation.

The optimal layout scheme of scenarios 1.4 and 2 are shown in Figs. 12–15. In Figs. 13 and 15, the white rectangle framed by the dotted line is the cable (or WT) array area. The lines with different colors represent different types of submarine cables. The thickness of the line reflects the amount of electricity being transported.

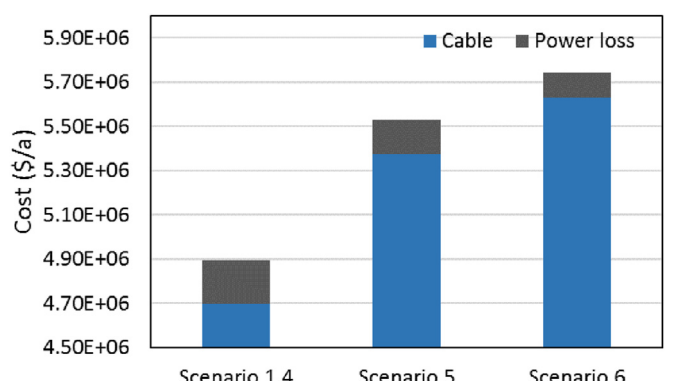


Fig. 19. The results of costs (Scenarios 1.4, 5, 6).

From the figures, WTs in Scenario 1.4 tend to be put in a line perpendicular to the most frequent wind. This distribution is conducive to maximize the use of wind energy to increase power generation and minimize the wake loss caused by WTs distribution. However, in Scenario 2, the locations of WTs tend to be along the direction of the maximum frequency wind. The reason for this distribution is that the distance between WTs is much longer than that in Scenario 1.4, which reduces the wake loss significantly. In other words, the longer distance weakens the influence of WTs distribution on wake loss. Meanwhile, it also means a longer submarine cable and more energy loss. A balance between power generation and cable investment & energy loss should be considered. For the locations of the offshore substation and onshore substation, if they are located at similar latitudes and the seabed is relatively flat, the cable length will be reduced, as well as the investment and operating costs, just like the export cable in Fig. 12.

5.3. Dimension comparison

In Scenario 4, the seabed terrain is not taken into consideration. More specifically, the cable network model does not consider elevations of grids other than the obstacle area when optimizing the cable routing. Therefore, the differences between Scenario 1.4 and Scenario 4 are mainly associated with different 3D cable lengths and obstacle-avoiding. Note that the analysis for the consideration of seabed terrain does not apply to floating wind farms. It can be seen a decrease with 263.86 thousand dollars a year on benefits than Scenario 1.4. Meanwhile, cable cost and energy loss cost are also increased. Figs. 16 and 17 display the layouts of Scenario 4. It is found that the seabed terrain in Scenario 1.4 has a more obvious impact on the layout of WTs. More WTs in Fig. 13 tend to be concentrated in flat areas. It is similar in Fig. 15 which also considers the seabed terrain. Regarding the influence of seabed terrain on cable routing, array cables are basically laid along contour lines to reduce the increase in length and construction difficulties caused by undulating terrain, as shown in Fig. 15. In Figs. 13 and 17, the export cables directly pass through the areas with large undulations on the seabed without bypassing these obstacles. This is because the height difference of the obstacles in the established case study is much smaller than the increased length by the detour. However, it does not mean that the seabed terrain can be ignored. If the seabed is seriously undulating, 3D optimization will become

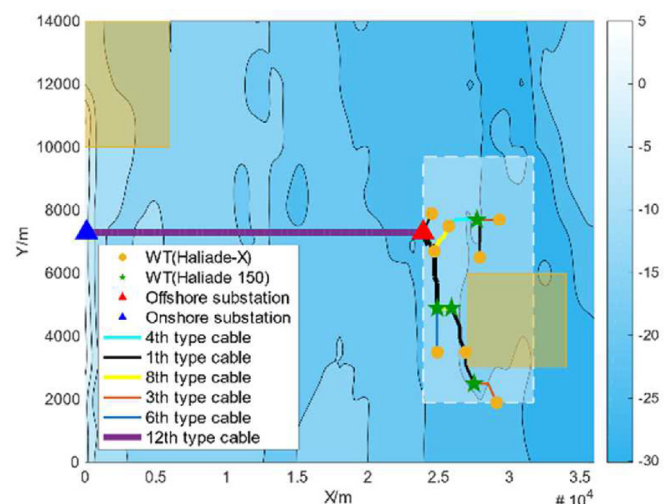


Fig. 21. 2D layout of Scenario 5.

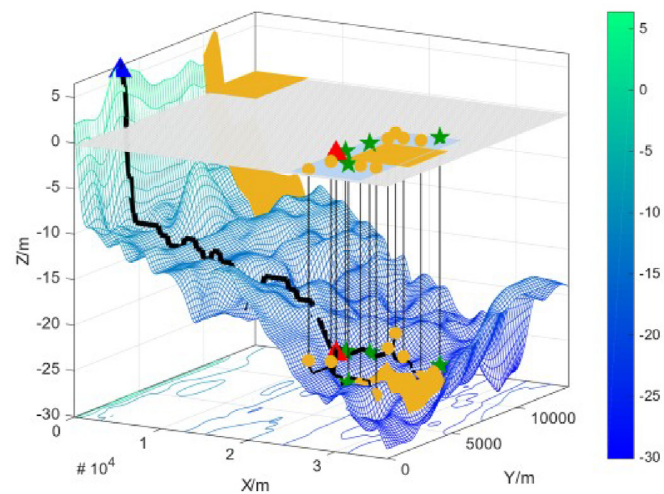


Fig. 22. 3D layout of Scenario 6.

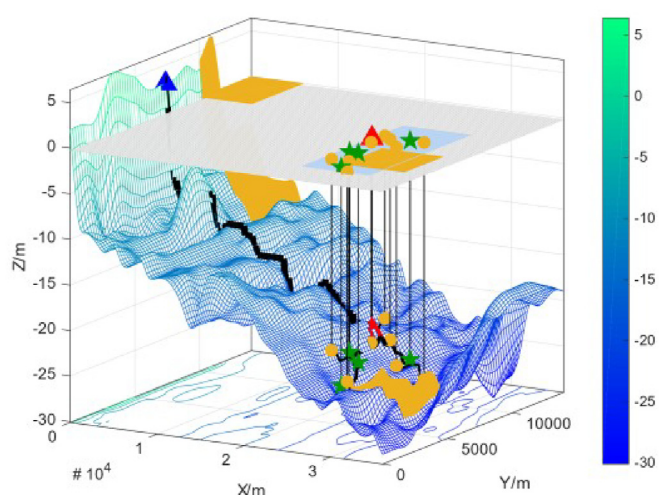


Fig. 20. 3D layout of Scenario 5.

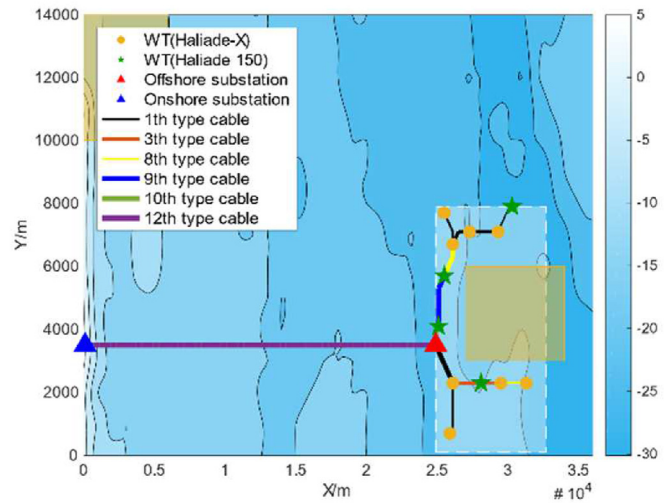


Fig. 23. 2D layout of Scenario 6.

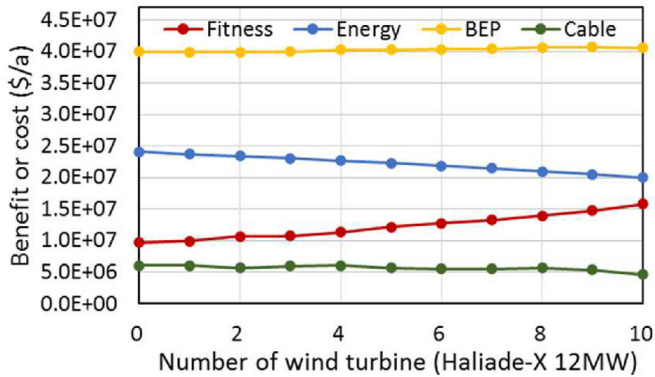


Fig. 24. The benefits and costs with different numbers of Haliade-X wind turbines.

more practical. In short, 3D optimization can bring more benefits to the offshore wind farm and reduce difficulties in the actual construction stage.

5.4. Site selection and WT type comparison

5.4.1. Comparison results

This section compares the effect of WT array location optimization and different WT types on the total annual benefit of the wind farm. As shown in Table 6 and Fig. 18, when the WT array location is optimized in Scenario 6, the optimal annual benefit is 76.79 thousand dollars more than Scenario 5 whose location is fixed. This illustrates the necessity of the site optimization of the WT array area. In Fig. 18, the annual benefits of scenarios 5–6 are significantly smaller than Scenario 1.4, as well as the power generation. For scenarios 5–6, the costs of cable and power loss are both higher than Scenario 1.4 (see Fig. 19). Therefore, under the same total installed capacity, the installation of WTs with larger rated power is more conducive to the profitability of the wind farm. Also, the ability of the proposed model to optimize the layout of multi-type WTs is verified.

Figs. 20–23 are the layout visualizations of scenarios 5 and 6. In each scenario, there are eight Haliade-X 12 MW WTs and four Haliade 150 6 MW WTs. The total installed capacity is equal to Scenario 1.4. It is observed that the latitudes of substations are identical in both scenarios. This is similar to Scenario 1.4, which helps reduce the length of the export pipeline and energy loss during transmission. Compared to Figs. 13 and 23, when the total number of WTs increases compared with Scenario 1.4, the total cable length required to connect more WTs becomes longer. According to the results in Table 6, the cable costs in the two scenarios increase by 14.41% and 19.82% compared to Scenario 1.4. This is mainly caused by the distance constraint (Eq. (44)) between WTs. On the other hand, from Fig. 21, the cable length is increased due to the detour to avoid the obstacle area. However, in Scenario 6, the positions of the WTs array area and WTs can be optimized at the same time, thereby reducing the influence of the obstacle area on the layout. The cables in Scenario 6 do not need to avoid the obstacle area. Moreover, the power generation of Scenario 6 is more than Scenario 5. Therefore, it is better than Scenario 5. This proves the practical significance of considering the site selection of the WTs array area for the OWFL problem.

5.4.2. Sensitivity analysis

To further explore the impact of the number of large rated-power WTs on the annual benefit of the offshore wind farm, a sensitivity analysis is established. The variety of several targets

with the number of Haliade-X (12 MW) WTs is shown in Fig. 24. When the number of Haliade-X WTs increases by one, the number of Haliade 150 (6 MW) WTs must be reduced by two to ensure the same total installed capacity. Therefore, the total number of variables decreases as the number of Haliade-X WTs increases. To achieve a fair comparison, the population size of GA and improved ACO are proportional to the total number of variables. The results show that fitness is increasing as the Haliade-X WTs number increases. One reason is that the effectiveness of Haliade-X is higher than Haliade 150. The parameters in Table 2 explain this, the wind speed range (3.5–28 m/s) of the power generation of Haliade-X is larger than Haliade 150 (3–25 m/s). So, B^{EP} basically shows an upward trend in Fig. 24. On the other hand, energy cost and cable cost decrease when the number of Haliade-X WTs increases. When the total installed capacity is the same, the larger the rated power of a single WT, the lower the unit costs of investment, installation and operation. Besides, the reduction in WTs number will shorten the total length of submarine cables, resulting in less energy loss and higher space utilization. In summary, the application of WTs with large rated power can improve the efficiency of the wind farm.

6. Conclusion

In this paper, an integrated model is introduced describing problems of site selection, multiple type WTs layout and cable network (array cable and export cable). The model is universal and fully functional. The main novelty contributions of this work are (a) the realization of the simultaneous optimization with multiple subproblems; (b) the proposal of GIS-based 3D obstacle-avoiding layout methodology for the offshore wind farm; (c) a hybrid algorithm coupling GA-IACO, graph theory algorithm and LP solver in Matlab is achieved successfully. The proposed methodology has not been applied to a real project, but it has been validated through a proposed case study based on a real wind farm.

From the results, the simultaneous optimization of multiple sub-problems can increase the annual benefit by hundreds of thousands or even millions of dollars in the lifetime of the offshore wind farm. The advantages and practicality of the proposed model and algorithm are illustrated. Besides, the seabed terrain, which is innovatively considered, not only influences the relative positions of WTs and substations but also directly affects the submarine cable routing. It is a practical factor that cannot be ignored. Due to the complexity of the highly integrated design problem, these optimal layout schemes cannot be produced manually. This work is helpful for the practical OWFL problem. It is found that there is a balance between power generation and costs of cable and energy loss, so, further research interests should include multi-objective optimization considering more realistic factors such as policy and environmental protection.

The proposed model also has some limitations. Firstly, for the cost model, some foundation costs are not considered, such as the cost of the submarine support of wind turbines. The submarine support cost of wind turbines is related to the elevation of the seabed, which can further prove the importance of considering the 3D layout. Secondly, the proposed model does not include some practical factors, such as fatigue loads for the wake loss model and environmental effects including noise, birds, etc. In the future, these factors can be integrated into the proposed model to improve the quality and practicality of the methodology.

CRediT authorship contribution statement

Yan Wu: Methodology, Validation, Writing – original draft. **Tianqi Xia:** Methodology. **Yufei Wang:** Conceptualization, Writing

– review & editing, Supervision, Funding acquisition. **Haoran Zhang:** Conceptualization, Writing – review & editing. **Xiao Feng:** Supervision. **Xuan Song:** Methodology. **Ryosuke Shibasaki:** Supervision.

Declaration of competing interest

The authors declare that they have no known competing financial interests or personal relationships that could have appeared to influence the work reported in this paper.

Acknowledgments

(1). Financial support from the National Natural Science Foundation of China under Grant (No. 22022816 and 22078358) is acknowledged.

(2). The support provided by the China Scholarship Council (CSC) during a visit by Yan Wu to the University of Tokyo is gratefully acknowledged.

References

- [1] L. Joyce, Z. Feng, in: Global Wind Report 2019, Global Wind Energy Council, 2020. <https://gwec.net/global-offshore-wind-report-2020/>.
- [2] M.A. Lackner, C.N. Elkinton, An analytical framework for offshore wind farm layout optimization, *Wind Eng.* 31 (1) (2007) 17–31.
- [3] B. Pérez, R. Minguez, R. Guanche, Offshore wind farm layout optimization using mathematical programming techniques, *Renew. Energy* 53 (2013) 389–399.
- [4] R. Brogna, et al., A new wake model and comparison of eight algorithms for layout optimization of wind farms in complex terrain, *Appl. Energy* 259 (2020) 114189.
- [5] C.L. Archer, et al., Review and evaluation of wake loss models for wind energy applications, *Appl. Energy* 226 (2018) 1187–1207.
- [6] N.O. Jensen, A Note on Wind Generator Interaction, 1983.
- [7] G.C. Larsen, A Simple Wake Calculation Procedure, Risø National Laboratory, 1988.
- [8] S. Frandsen, et al., Analytical modelling of wind speed deficit in large offshore wind farms, *Wind Energy* 9 (1–2) (2006) 39–53.
- [9] M. Bastankhah, F. Porté-Agel, A new analytical model for wind-turbine wakes, *Renew. Energy* 70 (2014) 116–123.
- [10] S. Xie, C. Archer, Self-similarity and turbulence characteristics of wind turbine wakes via large-eddy simulation, *Wind Energy* 18 (10) (2015) 1815–1838.
- [11] N.S. Ghaisas, C.L. Archer, Geometry-based models for studying the effects of wind farm layout, *J. Atmos. Ocean. Technol.* 33 (3) (2016) 481–501.
- [12] L.J. Vermeer, J.N. Sørensen, A. Crespo, Wind turbine wake aerodynamics, *Prog. Aero. Sci.* 39 (6) (2003) 467–510.
- [13] A. Crespo, J. Hernández, Turbulence characteristics in wind-turbine wakes, *J. Wind Eng. Ind. Aerod.* 61 (1) (1996) 71–85.
- [14] S.T. Frandsen, M.L. Thøgersen, Integrated fatigue loading for wind turbines in wind farms, in: European Seminar Offshore Wind Energy in Mediterranean and Other European Seas, 2000. Roma.
- [15] M.L. Fischetti, John Josef, Anders Bech Borchersen, A Mixed-Integer Linear Programming approach to wind farm layout and inter-array cable routing, in: American Control Conference, 2015. Chicago, IL, USA.
- [16] S. Song, et al., Integrated optimization of offshore wind farm layout design and turbine opportunistic condition-based maintenance, *Comput. Ind. Eng.* 120 (2018) 288–297.
- [17] C. Maienza, et al., A life cycle cost model for floating offshore wind farms, *Appl. Energy* 266 (2020) 114716.
- [18] J. Serrano Gonzalez, et al., Optimal wind-turbine micro-siting of offshore wind farms: a grid-like layout approach, *Appl. Energy* 200 (2017) 28–38.
- [19] S. Dutta, T.J. Overbye, Optimal wind farm collector system topology design considering total trenching length, *IEEE Trans. Sustain. Energy* 3 (3) (2012) 339–348.
- [20] H. Peng, H. Weihao, Z. Chen, Offshore substation locating in wind farms based on prim algorithm, in: 2015 IEEE Power & Energy Society General Meeting, 2015.
- [21] P. Hou, et al., Overall optimization for offshore wind farm electrical system, *Wind Energy* 20 (6) (2017) 1017–1032.
- [22] A.C. Pillai, et al., Offshore wind farm electrical cable layout optimization, *Eng. Optim.* 47 (12) (2015) 1689–1708.
- [23] P. Hou, et al., Combined optimization for offshore wind turbine micro siting, *Appl. Energy* 189 (2017) 271–282.
- [24] A. Cerveira, et al., Optimal cable design of wind farms: the infrastructure and losses cost minimization case, *IEEE Trans. Power Syst.* 31 (6) (2016) 4319–4329.
- [25] A. Wędzik, T. Siewierski, M. Szypowski, A new method for simultaneous optimizing of wind farm's network layout and cable cross-sections by MILP optimization, *Appl. Energy* 182 (2016) 525–538.
- [26] Y. Wu, et al., A design methodology for wind farm layout considering cable routing and economic benefit based on genetic algorithm and GeoSteiner, *Renew. Energy* 146 (2020) 687–698.
- [27] M. Fischetti, D. Pisinger, Optimizing wind farm cable routing considering power losses, *Eur. J. Oper. Res.* 270 (3) (2018) 917–930.
- [28] A. Klein, D. Haugland, Obstacle-aware optimization of offshore wind farm cable layouts, *Ann. Oper. Res.* 272 (1) (2019) 373–388.
- [29] D. Jiang, et al., A fuzzy evidential reasoning based approach for submarine power cable routing selection for offshore wind farms, *Ocean Eng.* 193 (2019) 106616.
- [30] P. Hou, et al., A review of offshore wind farm layout optimization and electrical system design methods, *J. Mod. Power Syst. Clean Energy* 7 (5) (2019) 975–986.
- [31] R. Shakoor, et al., Wake effect modeling: a review of wind farm layout optimization using Jensen's model, *Renew. Sustain. Energy Rev.* 58 (2016) 1048–1059.
- [32] Y. Chen, et al., Wind farm layout optimization using genetic algorithm with different hub height wind turbines, *Energy Convers. Manag.* 70 (2013) 56–65.
- [33] X. Gao, et al., Wind turbine layout optimization using multi-population genetic algorithm and a case study in Hong Kong offshore, *J. Wind Eng. Ind. Aerod.* 139 (2015) 89–99.
- [34] P. Hou, et al., Optimized placement of wind turbines in large-scale offshore wind farm using particle swarm optimization algorithm, *IEEE Trans. Sustain. Energy* 6 (4) (2015) 1272–1282.
- [35] S. Pookpunt, W. Ongsakul, Design of optimal wind farm configuration using a binary particle swarm optimization at Huasai district, Southern Thailand, *Energy Convers. Manag.* 108 (C) (2016) 160–180.
- [36] Y. Eroglu, S.U. Seçkiner, Design of wind farm layout using ant colony algorithm, *Renew. Energy* 44 (2012) 53–62.
- [37] A. Kusiak, Z. Song, Design of wind farm layout for maximum wind energy capture, *Renew. Energy* 35 (3) (2010) 685–694.
- [38] R. Srikanthapu, U. Vinatha, Combined approach based on ACO with MTSP for optimal internal electrical system design of large offshore wind farm, in: 2018 International Conference on Power, Instrumentation, Control and Computing, PICC), 2018.
- [39] R.A. Rivas, et al., Solving the turbine positioning problem for large offshore wind farms by simulated annealing, *Wind Eng.* 33 (3) (2009) 287–297.
- [40] S. Salcedo-Sanz, et al., Offshore wind farm design with the Coral Reefs Optimization algorithm, *Renew. Energy* 63 (2014) 109–115.
- [41] S. Rehman, S.S. Ali, S.A. Khan, Wind farm layout design using cuckoo search algorithms, *Appl. Artif. Intell.* 30 (10) (2016) 899–922.
- [42] P. Mittal, K. Kulkarni, K. Mitra, A novel hybrid optimization methodology to optimize the total number and placement of wind turbines, *Renew. Energy* 86 (2016) 133–147.
- [43] H. Zhang, et al., A hybrid computational approach for detailed scheduling of products in a pipeline with multiple pump stations, *Energy* 119 (2017) 612–628.
- [44] T.R. Ayodele, et al., A multi-criteria GIS based model for wind farm site selection using interval type-2 fuzzy analytic hierarchy process: the case study of Nigeria, *Appl. Energy* 228 (2018) 1853–1869.
- [45] L. Castro-Santos, M.I. Lamas-Galdo, A. Filgueira-Vizoso, Managing the oceans: site selection of a floating offshore wind farm based on GIS spatial analysis, *Mar. Pol.* 113 (2020) 103803.
- [46] I. Katic, J. Højstrup, N.O. Jensen, A simple model for cluster efficiency, in: European Wind Energy Association Conference and Exhibition, 1986.
- [47] J.C. Bansal, P. Farswan, Wind farm layout using biogeography based optimization, *Renew. Energy* 107 (2017) 386–402.
- [48] S. Pookpunt, W. Ongsakul, Optimal placement of wind turbines within wind farm using binary particle swarm optimization with time-varying acceleration coefficients, *Renew. Energy* 55 (2013) 266–276.
- [49] K. Yang, et al., Wind farm layout optimization for wake effect uniformity, *Energy* 183 (2019) 983–995.
- [50] M. Abdulrahman, D. Wood, Investigating the Power-COE trade-off for wind farm layout optimization considering commercial turbine selection and hub height variation, *Renew. Energy* 102 (2017) 267–278.
- [51] G. Gualtieri, A novel method for wind farm layout optimization based on wind turbine selection, *Energy Convers. Manag.* 193 (2019) 106–123.
- [52] J. Chen, F. Wang, K.A. Stelson, A mathematical approach to minimizing the cost of energy for large utility wind turbines, *Appl. Energy* 228 (2018) 1413–1422.
- [53] G. Gualtieri, Comparative analysis and improvement of grid-based wind farm layout optimization, *Energy Convers. Manag.* 208 (2020) 112593.
- [54] S. Rajper, I.J. Amin, Optimization of wind turbine micrositing: a comparative study, *Renew. Sustain. Energy Rev.* 16 (8) (2012) 5485–5492.
- [55] R. Jin, et al., Cable routing optimization for offshore wind power plants via wind scenarios considering power loss cost model, *Appl. Energy* 254 (2019) 113719.
- [56] ABB. XLPE Land Cable Systems User's Guide.
- [57] L. Wang, et al., An optimization method based on random fork tree coding for the electrical networks of offshore wind farms, *Renew. Energy* 147 (2020) 1340–1351.
- [58] W. Li, E. Özcan, R. John, Multi-objective evolutionary algorithms and hyper-heuristics for wind farm layout optimisation, *Renew. Energy* 105 (2017) 473–482.
- [59] D. Wilson, et al., Evolutionary computation for wind farm layout optimization, *Renew. Energy* 126 (2018) 681–691.

- [60] M. Dorigo, V. Maniezzo, A. Colorni, Positive feedback as a search strategy, in: Tech rep., 91-016, Dip Elettronica, Politecnico di Milano, Italy, 1999.
- [61] M. Dorigo, G. Di Caro, L.M. Gambardella, Ant algorithms for discrete optimization, Artif. Life 5 (1999) 137–172.
- [62] <https://www.delmarvanow.com/story/news/local/delaware/2018/10/25/delawares-offshore-wind-energy-maryland-offshore-wind-energy-ocean-city-delmarva/1458605002/>.
- [63] <https://www.ncdc.noaa.gov/>
- [64] <https://download.gebco.net>.

Nomenclature

Main Abbreviations

ACO: Ant Colony Optimization
 AEP: Annual Energy Production
 COE: The Cost of Energy
 GA: Genetic Algorithm
 GIS: Geographic Information System
 IACO: Improved Ant Colony Optimization
 LP: Linear Programming
 MINLP: Mixed-Integer Nonlinear Programming
 MST: Minimum Spanning Tree
 OWFL: Offshore Wind Farm Layout
 PSO: Particle Swarm Optimization
 SAA: Simulated Annealing Algorithm
 WT: Wind Turbine
 2D: Two-dimensional
 3D: Three-dimensional

Indices and Sets

D : ID set of wind directions
 P : ID set of all types of cables
 S : ID set of wind speeds
 V : ID set of all the vertexes in the whole given grided area
 V^A : ID set of all the WTs, offshore substation and onshore substation, $V^A = V^T \cup V^R = V^{WT} + V^R$
 V^{AC} : ID set of the vertexes (potential locations of WTs and offshore substation) in the array cable area
 V^C : ID set of the vertexes in the connected graph
 V^{EC} : ID set of the vertexes (potential locations of offshore and onshore substations) in the export cable area
 V^R : ID set of the offshore and onshore substations
 V^T : ID set of the vertexes in the minimum spanning tree, $V^T = V^C$
 V^{WT} : ID set of all the WTs
 Y : The set of serial numbers of all years in the life cycle

Input Parameters

b_i : Binary parameters indicate whether the i th node is an obstacle
 c_i : Original scale parameter of the wind speed distribution at i th WT
 c_p^c : Unit price of type p cable, \$/km

c_p^d : Distance between the axis of a conductor and the center type p cable, mm

c^e : Electricity price, \$(kWh)

c^{OPS} : Investment cost per offshore substation, \$

c^{OM} : Operation and maintenance cost per turbine, \$/a

c^{ONS} : Investment cost per onshore substation, \$

c^t : Unit cost of trench construction, \$/km

c_p^{WT} : Investment cost per WT, \$

d^A : Diameter of armor, mm

d_p^{CS} : Conductor diameter with the sheath of type p cable, mm

es : Economies of scale

f : Frequency, Hz

h : Wind data collection height, m

h_i^{WT} : Hub height of i th WT, m

i_p^k : Current rating of type p cable, kA

k : Shape parameter of wind speed

n^{AC} : Grid number of array cable area

n^{ACMax} : Maximum start column number of the array cable area

n^{ACMin} : Minimum start column number of the array cable area

n^{ARMax} : Maximum start row number of the array cable area

n^{ARMin} : Minimum start row number of the array cable area

n^P : Number of wind direction bins

n^{ERMax} : Maximum row number of the export cable area

n^{OPS} : Number of offshore substations

n^{TE} : Edge number of the minimum spanning tree
 n^V : Number of all vertexes in the given grid
 n^{VAC} : Node number of gridded array cable area
 n^{Ve} : Number of wind speed bins
 n^{VEC} : Node number of gridded export cable area
 n^{VT} : Node number of the minimum spanning tree
 n^{WT} : WTs number
 n^Y : Wind farm lifetime, year
 $p^{d\theta}$: Probability density of wind direction
 p_u^R : Rated power output of u th node, MW
 $p_{u,v,i}^R$: Rated power output of i th node when routing the cable between u th WT and v th WT or substation, MW
 p_d^θ : Probability of d th wind direction interval
 r^A : Resistance of armor at maximum armor temperature, Ω/km
 r^{EA} : Reactance of sheath or screen, Ω/km
 r_p^{EA} : Inductive reactance of the cable, Ω/km
 r_p^{ES} : Conductor resistance of the cable, Ω/km
 r^{IF} : Inflation rate
 r^{IT} : Interest rate
 r^S : Resistance of sheath or screen at maximum operating temperature, Ω/km
 r_i^{WT} : Rotor radius of WTs, m
 u_p^R : Rated voltage of the type p cable, kV
 v : Observed wind speed at h , m/s
 v_i^{CL} : Cut-in wind speed, m/s
 v_i^{CO} : Cut-off wind speed, m/s
 v_i^R : Rated wind speed, m/s
 (x_i, y_i, z_i) : Coordinates of i th node in the gridded area
 z_0 : Surface roughness, m
 z_i^0 : Original depth of i th node in the gridded area
 z^M : Depth constant, m
 δ : Plenty factor, \$
 n_i^{WT} : Power coefficient of i th WT
 κ_i : Wake spreading constant
 $\lambda_{1,p}$: Sheath loss factor
 $\lambda_{2,p}$: Armor loss factor
 θ : Wind directions
 ρ : Air density, kg/m^3
 ω : Angular frequency rad/s
 $\cos \phi$: Power factor requirement at the grid coupling point

Decision variables

N^{Col} : Integer variable refers to the start column of the array cable area in the whole given sea area
 N^{OPS} : Integer variable refers to the location of the offshore substation
 N^{ONS} : Integer variable refers to the location of the onshore substation
 N^{Row} : Integer variable refers to the start row of the array cable area in the whole given sea area
 N_i^{WT} : Integer variable refers to the location of each WT

Intermediate variables

$A_{i,j}^{overlap}$: The overlap area between rotor swept area of i th WT and the expanded wake area of the upstream j th WT, m²
 A_i^R : Rotor swept area of i th WT, m²
 $B_{i,j}$: Binary variables indicate whether the variables meet the constraints
 $B_{u,v,i,j}^{AC}$: Binary variables indicate whether there is a cable between two nodes in the array cable area
 $B_{u,v,i,j}^{EC}$: Binary variables indicate whether there is a cable between two nodes in the export cable area
 B^{EP} : Annual electricity production benefit, \$/y
 B^{NI} : Annual economic benefit (net income), \$/y
 B^{PV} : Total plenty value, \$/y
 C_i : The real scale parameter of the wind speed distribution at i th WT
 C_{cable} : Cable cost, \$/y
 C_{energy} : Energy production cost, \$/y
 C_{loss} : Energy loss cost, \$/y
 C_i^T : Thrust coefficient of i th WT
 $D_{i,j}$: The distance between every two turbines following the wind direction 0
 $D_{i,j}^{WR}$: The distance between the centers of the wake and turbine rotor, m.
 H^F : Annual average full-load hours for a specified wind farm, hour
 $I_{i,j}^R$: Rated current of each cable segment, kA
 $N_{i,j}^C$: Cable number between i th node and j th node

P_i : Power generation of ith WT, MW	V_{ij} : Wind speed at ith WT after being affected by jth WT, m/s
P_{cv}^i : Cumulative probability density of the wind speed	V_i^{Def} : Total wind speed deficit at ith WT
P_{dv}^i : Probability density of the wind speed	V_{ij}^{Def} : Wind speed deficit caused by jth WT to ith WT
P_{ij}^{loss} : Energy loss between ith WT and jth WCT MW·h	$W_{u,v}^C$: The total 3D length between uth node and vth node in $G(V^C, E^C, W^C)$, m
P_{ij}^R : Rated power of each cable segment between ith node and jth node, MW	$W_{u,v}^R$: The total 3D length between uth node and vth node in $T(V^R, E^R, W^R)$, m
$P_{u,u,ij}^R$: Rated power between ith node and jth node when routing the cable between uth WT and vth WT or substation, MW	$W_{u,v}^T$: The total 3D length between uth node and vth node in the minimum spanning tree $T(V^T, E^T, W^T)$, m
R_j^W : Downstream rotor radius caused by jth WT, m	θ_{ij}^R : Rotor intersection arc (ith WT)
R_{ij}^W : Wake radius caused by jth WT at the location of ith WT, m	θ_{ij}^W : Angle of the wake intersection arc (jth WT)
V_i : Wind speed at the location of ith WT, m/s	